IL-7-mediated expansion of autologous lymphocytes increases CD8$^+$ VLA-4 expression and accumulation in glioblastoma models

Authors

1. Kirit Singh[1,2]
2. Kelly M. Hotchkiss[1,2]
3. Sarah L. Cook[1,2]
4. Pamy Noldner[3]
5. Ying Zhou[3]
6. Eliese M. Moelker[1,2]
7. Chelsea O. Railton[1,2]
8. Emily E. Blandford[1,2]
9. Bhairavy J. Puviindran[1,2]
10. Shannon E. Wallace[1,2]
11. Pamela K. Norberg[1,2]
12. Gary E. Archer[1,2]
13. Beth H. Shaz[3]
14. Katayoun Ayasoufi[1,2]
15. John H. Sampson[4]
16. Mustafa Khasraw[1,2†, *]
17. Peter E. Fecci[1,2,5†, *]

[1]The Preston Robert Tisch Brain Tumor Center at Duke University Medical Center, Durham, NC, US.

[2]Department of Neurosurgery, Duke University Medical Center, Durham, NC, US.

[3]The Marcus Center for Cellular Cures, Duke University Medical Center, Durham, NC, US.

[4]University of Colorado School of Medicine, Anschutz Medical Campus, Aurora, CO.

[5]Duke Center for Brain and Spine Metastasis.

*These authors contributed equally to the manuscript.

†Co-Corresponding Author: Mustafa Khasraw, M.D.

The Preston Robert Tisch Brain Tumor Center

Duke University | Box 3624, Durham, NC 27710

T +1 919.684.6173 | F +1 919.681.1697

mustafa.khasraw@duke.edu

†Co-Corresponding Author: Peter E. Fecci, M.D., Ph.D.,

The Preston Robert Tisch Brain Tumor Center

Duke University | Box 3050, Durham, NC 27710

T +1 919.681.8977 | F +1 919.684.9045

peter.fecci@duke.edu

Keywords

Immunotherapy; T cells; Cell migration/adhesion

Conflict-of-interest statement

1. KS reports grants paid to his institution and research contracts from Adaptin Bio, which has licensed intellectual property from Duke related to the use of Brain Bi-specific T cell Engagers (BRiTE) and combination autologous lymphocyte therapy.
2. KMH reports no relevant disclosures.
3. SLC reports grants paid to her institution from Immorna Therapeutics, Immvira Therapeutics.
4. PN reports no relevant disclosures.
5. YZ reports no relevant disclosures.
6. EMM reports no relevant disclosures.
7. COR reports no relevant disclosures.

8. EEB reports no relevant disclosures.
9. BP reports no relevant disclosures.
10. SW reports no relevant disclosures.
11. PKN reports no relevant disclosures.
12. GEA reports no relevant disclosures.
13. BHS reports no relevant disclosures.
14. KA reports no relevant disclosures.
15. JHS reports an equity interest in Istari Oncology, which has licensed intellectual property from Duke related to the use of poliovirus and D2C7 in the treatment of glioblastoma. JHS is an inventor on patents related to BRiTE, PEP-CMV DC vaccine with tetanus, as well as poliovirus vaccine and D2C7 in the treatment of glioblastoma.
16. MK reports grants paid to his institution, or contracts from BMS, AbbVie, BioNTech, CNS Pharmaceuticals, Daiichi Sankyo Inc., Immorna Therapeutics, Immvira Therapeutics, JAX lab for genomic research, and Personalis Inc. MK also received consulting fees from AnHeart Therapeutics, George Clinical, Manarini Stemline, and Servier and is on a data safety monitoring board for BPG Bio.
17. PEF reports funding from a Cancer Research Institute (CRI) Arash Ferdowsi Lloyd J.Old STAR Award.

Abstract

The efficacy of T cell-activating therapies against glioma is limited by an immunosuppressive tumor microenvironment and tumor-induced T cell sequestration. We investigated whether peripherally infused non-antigen specific autologous lymphocytes (ALT) could accumulate in intracranial tumors. We observed that non-specific autologous $CD8^+$ ALT cells can indeed accumulate in this context, despite endogenous T cell sequestration in bone marrow. Rates of intratumoral accumulation were markedly increased when expanding lymphocytes with IL-7 compared to IL-2. Pre-treatment with IL-7 ALT also enhanced the efficacy of multiple tumor-specific and non-tumor-specific T cell-dependent immunotherapies against orthotopic murine and human xenograft gliomas. Mechanistically, we detected increased VLA-4 on mouse and human $CD8^+$ T cells following IL-7 expansion, with increased transcription of genes associated with migratory integrin expression (*CD9)*. We also observed that IL-7 increases *S1PR1* transcription in human $CD8^+$ T cells, which we have shown to be protective against tumor-induced T cell sequestration. These observations demonstrate that expansion with IL-7 enhances the capacity of ALT to accumulate within intracranial tumors, and that pre-treatment with IL-7 ALT can boost the efficacy of subsequent T cell-activating therapies against glioma. Our findings will inform the development of future clinical trials where ALT pre-treatment can be combined with T cell-activating therapies.

Brief Summary

T cell immunotherapies are limited by few T cells in glioma. Adoptively transferred lymphocytes expanded with IL-7 exhibit increased VLA-4 expression and accumulate in tumors.

Introduction

T cell-activating immunotherapies, such as immune checkpoint blockade (ICB), require functional T cells at the tumor site to be effective (1-3). Unfortunately, intracranial tumors are harbored within the immunologically distinct central nervous system (CNS) and sit shielded by an immunosuppressive tumor micro-environment (TME) and the blood-brain barrier (BBB) (4). We have shown that CNS tumors, such as glioblastoma, also possess the unique ability to sequester naïve T cells within bone marrow (5), limiting their access to the TME. Likewise, we have more recently described a central role for tumor-associated macrophages (TAM) in driving glioma-infiltrating T cells towards a terminally exhausted state (6), limiting their antitumor capacities. Accordingly, high-grade gliomas possess low numbers of tumor infiltrating lymphocytes (TILs (7)) and have proven minimally responsive to ICB in clinical trials (8-10). This paucity of functional TILs will similarly limit the therapeutic efficacy of newer synthetic therapies that rely on endogenous T cells, including brain bi-specific T cell engagers (BRiTEs) (11). Strategies for enhancing functional T cell presence within CNS tumors are needed.

Currently, strategies to increase T cell numbers in tumor include expanding the T cell pool intratumorally; encouraging T cell trafficking from the periphery; or adding T cells systemically. Each of these face major challenges. Expansion of local lymphocytes is limited by subsequent severe exhaustion amidst tumor-infiltrating $CD8^+$ T cells, making them less proliferative to stimulation (12). Recruitment of peripheral lymphocytes can be boosted by immunostimulatory cytokines (e.g., IL-7 (13) or IL-12 (14)), but peripheral cytokine administration can induce profound systemic toxicity (15-17). Local administration of cellular therapies or immunostimulatory cytokines is an alternative but requires an invasive procedure, limiting the potential for repeat administrations (18, 19). Ultimately, peripheral infusion of unmodified or CAR-T cells is an established and easily repeatable method of adding lymphocyte populations to tumors within the CNS (20, 21). Modifying this approach, then, we asked whether peripherally infused non-antigen specific autologous lymphocytes would accumulate in established CNS tumors and synergize with T cell-activating/ICB therapies.

Currently, cellular therapies such as adoptive lymphocyte transfer (ALT) typically use cytokines such as Interleukin-2 (IL-2) or IL-7 to support *ex vivo* T cell expansion (22). IL-2 skews lymphocytes towards a terminally differentiated T effector (T_{EFF}) phenotype. While T_{EFF} cells do express migratory integrins, they often have a short half-life once removed from culture (23, 24). IL-7, in turn, promotes homeostatic T cell expansion and expands the central memory T cell (T_{CM}) pool, leading to greater T cell persistence in vivo (25, 26). Peripheral administration of long-acting IL-7 has been shown to enhance T cell accumulation in murine glioma and boosts the efficacy of T cell engagers against solid tumors (13, 27). We

therefore sought to evaluate which growth factor might produce a cellular product with favorable BBB-penetrance and enhanced anti-tumor efficacy in models of established intracranial glioma.

Herein, we report that peripherally administered T cells (ALT) lacking antigen specificity accumulate in established murine intracranial tumors, despite tumor-imposed T cell sequestration in bone marrow. Rates of intratumoral accumulation are markedly increased when T cells are expanded with IL-7 (IL-7-ALT), which also increases the efficacy of accompanying immunotherapeutic platforms. We find that IL-7 increases expression of the migratory integrin Very Late Antigen-4 (VLA-4) on both mouse and human $CD8^+$ T cells, while VLA-4 blockade abrogates the enhanced accumulation of IL-7-ALT in tumors. Transcriptional analysis of hPBMCs expanded with IL-7 reveals upregulation of genes involved in integrin expression and tumor infiltration (*CD9, VLA-6, EPHA4).* Also upregulated is *S1PR1* (sphingosine-1-phosphate receptor 1, also described as S1P1), increased levels of which are known to avert T cell sequestration and license immunotherapeutic responses to glioma (5). These results provide a route to optimizing ALT expansion, as well as to using ALT as an immunotherapeutic adjunct.

Results

IL-7-expanded CD8$^+$ T cells demonstrate increased accumulation within orthotopic glioblastoma models despite endogenous T cell sequestration in bone marrow

Though peripherally administered, activated autologous T cells have been shown to cross the BBB under physiologic conditions (28), their ability to enter the CNS in the setting of tumor-directed T cell sequestration was unclear. Previous work by our group established that sequestration predominantly impacts naïve T cells (endogenous or ALT), while memory T cells are largely unperturbed (5). We therefore began by examining the rate of CNS tumor accumulation for *ex vivo*-expanded non-specific autologous T cells.

First, we developed T cell expansion processes that skewed phenotypes towards effector (T_{EFF}, CD44^{high}CD62L^{low}) or central memory (T_{CM}, CD44^{high}CD62L^{high}) subsets. Expansion of T cells with either 100IU/mL IL-2 or 20ng/mL IL-7 was chosen to enrich for CD8$^+$ T_{EFF} or CD8$^+$ T_{CM} phenotypes, respectively, based on prior experience and published protocols (22, 29, 30). Following expansion, flow cytometry was performed to assess the makeup of the ALT product pre-administration (gating and expansion strategy in Figure S1, A and B). *Ex vivo* expansions with both IL-2 and IL-7 yielded a cellular product of >95% CD3$^+$ cells (Figure S1C) which predominantly consisted of CD8$^+$ T cells (~80%, Figure S1D). The IL-2-ALT product was preferentially skewed towards T_{EFF} (Figure S1E) while the IL-7-ALT product skewed towards T_{CM} (Figure S1F). Few naïve CD8$^+$ T cells (T_N, CD44^{low}CD62L^{high}) were present at the end of expansion with either cytokine (Figure S1G).

To establish the trafficking capabilities of non-specific CD45.1$^+$ T cells in the setting of tumor, we intracranially implanted CT2A stably transfected with the glioma-specific neoantigen Epidermal Growth Factor Receptor variant III (EGFRvIII) into congenic CD45.2$^+$ C57/BL6 mice. CT2A is syngeneic on the C57 background and exhibits high heterogeneity, stemness, and resistance to therapy (31). We have also previously described tumor-induced T cell sequestration in bone marrow using this model (5).

After tumors were well-established at 13 days, mice were given a single ALT of either IL-2 or IL-7-expanded CD45.1$^+$ T cells (Figure 1A). Following ALT, tumor and bone marrow were collected daily from separate mice over 4 days. Flow cytometry was used to measure changes to the viable exogenous (CD45.1$^+$) and endogenous (CD45.2$^+$) CD3$^+$ T cell

compartment (flow gating in Figure S2A). By 48-hours post administration, we detected an increased proportion of the IL-7-ALT dose within tumor compared to IL-2-ALT. (Figure 1B, IL-7-ALT vs IL-2-ALT in tumor, $p<0.05$*). No significant difference between dose proportions in bone marrow was seen at the same timepoint (Figure 1B, $p=0.8172$). Examination of intratumoral T cells over time found that accumulation rates for IL-7-ALT $CD8^+$ but not $CD4^+$ lymphocytes were significantly greater than for IL-2-ALT. In both groups, endogenous $CD8^+$ T cell populations in tumor declined (time course shown for $CD4^+$ T cells in Figure 1C, $CD8^+$ T cells in Figure 1D. 48-hour IL-7-ALT $CD8^+$ T cells 31.24x vs IL-2-ALT 4.14x $p<0.01$**, 72-hour IL-7-ALT $CD8^+$ T cells 42.2x vs IL-2-ALT 5.88x, $p<0.01$**). Counts of IL-7-ALT $CD8^+$ T cells in tumor were also increased compared to IL-2-ALT throughout, though differences were non-significant (Figure S2B).

Simultaneously, increases in endogenous $CD4^+$ and $CD8^+$ T cell populations in bone marrow were seen across groups over time ($CD4^+$ T cells in Figure 1E, $CD8^+$ T cells in Figure 1F). Greater fold-change increases in endogenous $CD4^+$ T cell accumulation in bone marrow were observed compared to $CD8^+$ T cells, in keeping with previous descriptions of tumor-induced $CD4^+$ T cell sequestration (endogenous $CD4^+$ fold-change of 2.69x vs $CD8^+$ T cells fold change of 1.76x at 72-hr observation point (5, 32, 33)). ALT entry into bone marrow was also observed, although this was restricted to the $CD8^+$ population. Rates of ALT accumulation in bone marrow did not differ between expansion conditions (Figure 1F, non-adjusted IL-7-ALT $CD8^+$ T cell counts in Fig. S2C). Increases in spleen weights were also seen following ALT, before a subsequent precipitous decline below baseline (time course in Figure 1G). We concluded then that non-antigen specific, exogenously administered $CD8^+$ T cells can indeed accumulate within glioma despite tumor-imposed T cell sequestration, with IL-7-ALT accumulating intratumorally at a greater rate than IL-2-ALT.

IL-7-ALT synergizes with T cell-centric immunotherapies in orthotopic glioma models

We next examined whether IL-2 or IL-7 ALT would each enhance survival when combined with T cell-activating immunotherapies. In a first set of experiments, we combined each ALT with EGFRvIII-BRiTE in a U87 xenograft model stably transfected with EGFRvIII (U87vIII). EGFRvIII-BRiTE is a bi-specific T cell engager possessing specificity for both the CD3 receptor and the glioma-specific antigen EGFRvIII (34). As EGFRvIII-BRiTE is fully humanized, we evaluated efficacy in a NOD scid gamma (NSG) mouse model reconstituted with either IL-7- or IL-2-expanded human (h)PBMCs. We observed that IL-7 ALT yielded a significant but modest survival benefit when combined with BRiTE, compared to the IL-2-ALT-BRITE combination (Figure 2A, $p<0.05$*). Interestingly, no differences between the two modalities were observed in vitro (Figure 2B).

Having observed a survival benefit with the combination of IL-7-ALT + BRITE, we looked to see how successfully IL-7-ALT might also combine with various checkpoint or T cell activity modifying therapies that typically have limited or no success in CT2A models (outline in Figure 2C). After CT2AvIII tumors established for 10 days, animals were treated with IL-7 ALT alone, or in combination with αCTLA-4 (antagonist), αPD-1 (antagonist) or α4-1BB (agonist) monoclonal antibodies. We observed a small trend toward prolonged survival when combining IL-7 ALT with αPD-1 therapy (2/6 mice surviving > 30 days, 0/6 with long term overall survival), but a significant increase in survival when combining IL-7-ALT + α4-1BB compared to IL-7-ALT only (Figure 2D, $p<0.05$*). We therefore selected the IL-7-ALT + α4-1BB combination approach for further experiments in this model and performed controlled survival studies using the same timing schematic as above (Figure 2E). We again found that IL-7-ALT + α4-1BB therapy yielded a significant survival benefit, this time compared to combination IL-2-ALT and α4-1BB ($p<0.05$*); α4-1BB alone ($p<0.05$*); either IL-2 or IL-7-ALT only (both $p<0.01$**); or to untreated controls ($p<0.01$**). Interestingly, while combination IL-7 ALT + αPD-1 therapy exhibited a limited survival benefit in the CT2AvIII glioma model (Figure 2D), greater efficacy was observed in mice bearing more immunogenic GL261 gliomas (35) (Figure 2F).

We likewise evaluated whether adding IL-7 ALT to clinically relevant checkpoint blockade therapy would result in toxicity. Body weights during and for two weeks following treatment were recorded in the GL261-bearing mice whose survival is depicted in Figure 2F. No differences between groups were seen (Figure 2G). To evaluate toxicity in greater detail, we performed acute toxicity studies in healthy mice receiving IL-7 + αPD-1 therapy, comparing against sham controls (outline shown in Figure S3A). Body weights again remained stable throughout (Figure S3B). Five days after treatment-end, blood, liver tissue, spinal cord and brain were taken to assess for liver function, changes in cellular architecture and potential demyelination. No significant difference in serum chemistry was seen between groups (Figure S3C). Review of brain and spinal cord by a board-certified veterinary pathologist also found no differences in terms of histological features, cellular architecture, or demyelination (representative photomicrographs in Figure S3, D and E). Regarding liver, no histopathologic abnormalities related to lymphocytic infiltration were noted in the sham group, though presumed peri-mortem acute hepatocellular apoptosis/necrosis without associated inflammation was seen in 2 of 5 animals. In the combination group, pathologist review identified small numbers of randomly distributed foci (1 to 4 per animal) of acute to subacute hepatocellular apoptosis/necrosis associated with a mixed lymphocytic infiltrate (representative photomicrographs in Figure S3F). While these findings were considered to be treatment-related effects, they were considered unlikely to indicate systemic toxicity given the unchanged liver function tests.

IL-7-expanded CD8$^+$ T cells accumulating in tumor exhibit both central and effector memory phenotypes

Frequent antigenic stimulation upregulates trafficking molecules on T_{CM} cells (36, 37), while T_{EFF} cells also upregulate migratory ligands such as LFA-1 and VLA-4, enhancing endothelial binding following activation (23, 24). We therefore evaluated the phenotypic makeup of exogenous T cells that entered the brain following ALT, as well as their expression of migratory integrins.

To begin, we intravenously administered CD45.1$^+$ IL-2-ALT or IL-7-ALT to CD45.2$^+$ mice with established (15-day) CT2AvIII tumors. Tumors were collected 3- and 48-hours post ALT (outline in Figure 3A). Again, we observed significantly enhanced accumulation of IL-7-ALT CD8$^+$ T cells compared to IL-2-ALT (Figure 3B, 3-hrs $p<0.01$**, 48-hrs $p<0.001$***). Similar to previous findings, ALT in tumor primarily consisted of CD8$^+$ T cells (Figure 3C, CD8$^+$ vs CD4$^+$ T cells, $p<0.0001$****). By the 48-hour timepoint, IL-7-ALT T cells made up approximately ~20% of all T cells in tumor, (Figure 3D, mean 18.8%, SD ±4.3%, n=5), while the fraction of T cells that consisted of IL-2-ALT in tumor was ~1% (mean 1.7%, SD ±1.5%, n=4).

Evaluating the phenotypic composition of the CD8$^+$ T cells infiltrating tumor, we observed that at 48-hours post ALT administration, the endogenous CD8$^+$ T cell phenotypes in tumor were similar, regardless of whether ALT was expanded with IL-2 or IL-7. Phenotypes consisted mainly of effector (T_{EFF}) cells (Figure 3E). Regarding administered (exogenous) ALT CD8$^+$ T cells, IL-2-ALT in tumor also pre-dominantly consisted of T_{EFF} cells, while IL-7-ALT consisted of a mixed central/effector (T_{CM}/T_{EFF}) population (Figure 3F). Naïve populations were negligible and did not vary between groups. Given this, we considered that enhanced entry or retention might be more characteristic of the T_{CM} population. However, we noted that the make-up of ALT in tumor was similar to the phenotypic make-up of the IL-2 and IL-7 ALT cell product pre-administration (IL-2-ALT in vitro (pre-administration) vs. in vivo (post-administration) in Figure 3G; IL-7-ALT in Figure 3H). This led us to consider instead whether the increased fraction of CD8$^+$ T_{CM} in tumor for the IL-7-ALT group simply reflected the composition of the pre-administration product.

To clarify, we compared accumulation of the CD8$^+$ T_{CM} and T_{EFF} subsets between both ALT groups. Both the IL-7-ALT CD8$^+$ T_{EFF} and T_{CM} subsets were present in tumor in significantly greater numbers than their IL-2-ALT counterparts (individual subsets for each ALT condition in Figures 3I and 3J, comparison between ALT conditions in Figure 3K, IL-7-

ALT vs IL-2-ALT T_{CM} and T_{EFF} p<0.0001****). We concluded that enhanced accumulation of IL-7-ALT CD8$^+$ T cells in tumor was more a feature of IL-7 expansion, and not reflective of T_{CM} phenotype.

Expansion with IL-7 upregulates expression of the pro-migratory integrin VLA-4 on murine CD8$^+$ T cells, which is required for enhanced intratumoral accumulation

To better understand the impact of IL-7 on T cell accumulation in tumor, we analyzed the expression of migratory integrins common to all lymphocytes (VLA-4, LFA-1) on exogenous T cells that entered the CNS using flow cytometry (gating strategy in Figure 4A). We observed that both the expression of the migratory integrin VLA-4 and the fraction of VLA-4^{Hi} cells was significantly increased amidst IL-7-ALT CD8$^+$ T cells arriving early in tumor compared to IL-2-ALT, though this difference subsided by the 48-hour sampling point (gMFI in Figure 4B, 3-hrs & 48-hrs p<0.01**, CD8$^+$ T cell VLA-4^{Hi} % in Figure 4C). Conversely, we saw increased LFA-1 expression on IL-2-ALT CD8$^+$ T cells compared to IL-7-ALT at the first sampling timepoint (Figure 4D, p<0.01** LFA-1 gating in Figure S4A). The percentage of CD8$^+$ LFA-1^{Hi} T cells was similarly high throughout for both conditions (Figure 4E). The pre-administration fraction of CD8$^+$ VLA-4^{Hi} T cells was also higher amidst the IL-7-ALT, while the fraction of pre-administration CD8$^+$ LFA-1^{Hi} T cells was similar between groups (CD8$^+$ VLA-4^{Hi} T cells in Figure 4F, CD8$^+$ LFA-1^{Hi} T cells in Figure 4G, technical repeats for each ALT condition shown).

To evaluate the impact of VLA-4 levels on T cell trafficking to tumor, we again used IL-7 to generate an ALT consisting of CD4$^+$ and CD8$^+$ T cells that had increased VLA-4 expression compared to baseline levels seen when expanding with IL-2 (VLA-4^{Hi} or VLA-4^{Lo} ALT, pooled ALT expression shown in Figure S4B). VLA-4^{Hi} or VLA-4^{Lo} ALT were then separately administered to animals with 15-day established CT2AvIII tumors, either alone or alongside a VLA-4 blocking antibody (BioXCell, 200μg intraperitoneally (IP)). VLA-4^{Hi} ALT CD8$^+$ T cells demonstrated significantly enhanced accumulation within tumor compared to VLA-4^{Lo} ALT, accumulation that was abrogated by co-administration of αVLA-4 (VLA-4^{Hi} vs VLA-4^{Lo}, p<0.05*; VLA-4^{Hi} vs αVLA-4 & VLA-4^{Hi}, p<0.05*, 3 pooled experiments shown, Figure 4H). Administration of αVLA-4 was also found to reduce the therapeutic efficacy of combination IL-7-ALT + α4-1BB seen in the CT2AvIII model. Here, we observed that IP αVLA-4 reduced survival in the combination therapy group from 54 to 30 days, similar to monotherapy groups, though these curves were not significantly different (IP α4-1BB only: 37 days, 3 pooled experiments shown, Figure 4I). Based on these findings, we concluded that: (1) IL-7 exposure increases the expression of VLA-4 on CD8$^+$ T cells and (2) VLA-4 expression and signaling are necessary for the enhanced accumulation of IL-7 ALT CD8$^+$ T cells in glioma.

Intratumoral lymphocytic VLA-4 and endothelial/pericytic VCAM-1 expression increase over time in glioma

While evaluating ALT VLA-4 expression, we noted that VLA-4 levels were consistently elevated over time on endogenous $CD8^+$ T cells in tumor (Figure 5A). Noting the role of VLA-4 in guiding T cells towards inflamed tissue (38), we first examined whether VLA-4^{Hi} T cells were unique to the tumor environment. We performed flow cytometry on various tissues (brain, spleen, bone marrow, lungs, and blood) in mice with established CT-2AvIII tumors or sham-injected controls (experimental outline in Figure 5B, gating strategy in Figure S5A). Animals did not receive ALT, allowing for evaluation of endogenous T cell VLA-4 expression without external influence. We again observed a significant increase to the VLA-4^{Hi} fraction amidst $CD8^+$ T cells, as well as to weight-adjusted VLA-4^{Hi} $CD8^+$ T cell counts in brain tumor tissue compared to all other compartments, as well as to brain from sham controls (fractions in Figure 5C, comparisons in Figure 5D, $p<0.0001$****, weight adjusted counts vs sham controls in Figure S5B, $p<0.01$**). VLA-4^{Hi} $CD8^+$ T cells in tumor were overwhelmingly T_{EFF} cells (Figure S5C). Outside of the tumor, VLA-4^{Hi} $CD8^+$ T cells were most commonly found in the bone marrow (Figure 5, C and D).

As glioblastoma is characterized by high levels of microvascular proliferation (39), we next evaluated if endothelial/pericytic VCAM-1 (VLA-4's ligand (40)) was also increased in tumor. Recent studies of T cell recruitment in other intracranial tumor models (i.e., melanoma) found negligible VCAM-1^+ endothelial or pericyte populations (41). To determine if VCAM-1^+ cells were present in the context of glioma, we collected brain tissue from mice with established intracranial CT2AvIII glioma or sham-controls. Both endothelial ($CD31^+CD13^-$) and pericyte ($CD31^-CD13^+$) populations were analyzed via flow cytometry (outline in Figure 5E, gating in Figure S5D). Here, we observed a similar frequency of expression of VCAM-1 on endothelial cells and pericytes on Day 12 of tumor growth (~45%$^+$), with similar levels also seen across tumor and sham (Figure 5F). However, as tumors progressed further, increasing proportions and counts of VCAM-1^+ endothelial cells and pericytes were observed in tumor compared to sham (Figure 5G, pericytes $p<0.05$*, endothelial cells $p<0.01$**, D17 weight adjusted counts in Figure 5, H and I respectively).

Given this, we questioned whether intratumoral T cell accumulation might be enhanced by blocking the VLA-4-VCAM-1 axis, and whether results would differ if blockade was administered systemically vs. intracranially. To evaluate, we implanted mice with CT2AvIII gliomas, and 13 days later administered αVLA-4 either intraperitoneally or intracranially. As free αVLA-4 antibody levels are 100-fold reduced in cerebro-spinal fluid (CSF) compared to serum following systemic

infusion (42), we selected dose levels of 200 µg αVLA-4 intraperitoneally and 2 µg intracranially to achieve approximately equivalent exposure (experiment outline in Figure 5J). First, we evaluated the impact of both intraperitoneal and intracranial αVLA-4 on intratumoral $CD8^+$ T cell VLA-4 expression and found that both suppressed VLA-4 levels on T cells, though this was only sustained when administering intraperitoneally (Figure S5E). Next, we evaluated intracranial counts of endogenous $CD4^+$ and $CD8^+$ T cell populations 24- and 72-hrs post αVLA-4 administration. Across treatment groups, no differences were seen at the 24-hour measurement point (Figure S5F). By 72-hours, however, intraperitoneal αVLA-4 had elicited reduced counts of both $CD4^+$ and $CD8^+$ T cells in tumors, even compared to non-tumor-bearing controls (24-hr intratumoral counts in Figure S5F, 72-hr counts in Figure 5K, intraperitoneal αVLA-4 vs sham, $CD4^+$ and $CD8^+$ T cells, $p<0.05$*). Conversely, intracranial αVLA-4 produced increases in accumulation of both populations within tumors by 72-hrs post administration, though this was only significant for $CD4^+$ T cells compared to sham controls (Figure 5K, intracranial αVLA-4 vs sham, $CD4^+$ T cells $p<0.05$*, $CD8^+$ T cells $p=0.068$).

We therefore further investigated the therapeutic potential for intracranial VLA-4 blockade. While increasing intratumoral T cell counts remains a central goal, VLA-4 is involved in immune synapse formation and T cell activation (43), making the net impact of its blockade unclear. To evaluate the effects of VLA-4 blockade on T cell activity, we performed in vitro co-culture cytotoxicity assays with CT2AvIII, T cells, and EGFRvIII-BRiTE. αVLA-4 antibody was added at escalating amounts to BRiTE at its EC_{50} dose (0.01µg/mL, dose-finding data in Figure S5G). The addition of αVLA-4 indeed inhibited the T cell anti-tumor cytotoxicity otherwise mediated by BRiTE (Figure 5L). Thus, while intracranial αVLA-4 may enhance intratumoral T cell accumulation, there appears to be a negative impact on anti-tumor cytotoxicity.

IL-7 expansion of hPBMCs from both healthy volunteers and patients with glioblastoma upregulates lymphocyte VLA-4 expression

We therefore returned to further investigate our initial IL-7-ALT method for enhancing T cell numbers in tumor. To determine the clinical translatability of our approach, we sought to determine whether a) leukapheresis products from patients with glioblastoma would respond / expand to the same extent as those from healthy controls, and b) similar changes to VLA-4 expression and T cell migratory potential would occur when expanding human T cells in the presence of IL-7.

To permit relevant comparisons, we obtained leukapheresis products from healthy volunteers and patients with glioblastoma who had given written consent to provide PBMCs for the purposes of T cell expansion. An overview of donor

demographics and pathology is shown in Table 1. Median ages across groups were similar (controls 54.3 yrs (range 43.3–55.4) vs glioblastoma 58.7 yrs (range 37.4–63.3)) with a 2:1 M:F ratio in both groups. Of the glioblastoma samples, 5 of 6 were collected from patients who had previously received dexamethasone.

Samples from control and glioblastoma groups were thawed and activated via αCD3/αCD8 stimulation. Cultures were maintained for 14 days in media supplemented with 300 IU/mL IL-2 (based on prior protocols (44)) or 20 ng/mL IL-7. After expansion, cell counts, phenotypes, activation levels and VLA-4 expression were evaluated (flow gating and schematic in Figure S6, A and B). While both IL-7 and IL-2 were capable of independently supporting T cell proliferation (Figure 6A), IL-2 produced greater T cell yields for both control and GBM leukapheresis samples (Figure S6C). Perhaps surprisingly, no significant difference between control and glioblastoma T cell expansion rates were observed. The final expanded product consisted of ~95% $CD3^+$ T cells across all groups (Figure S6D). IL-7 expansion skewed significantly more towards $CD4^+$ T cells (~60:40 ratio of $CD4^+$:$CD8^+$ T cells), whereas IL-2 skewed more towards $CD8^+$ T cells ($CD4^+$:$CD8^+$ T cells ~ 33:66, Figure 6, B-D). On more specific phenotyping of memory and effector subsets, we observed that T_{EFF} ($CD45RO^-$ $CD45RA^+CD95^+CCR7^-$) and T Effector Memory ($T_{EM,}$ $CD45RO^+CD45RA^-CD62L^-CCR7^-$) fractions were similar across the IL-2 and IL-7 expansion groups (T_{EFF} in Figure S6E, T_{EM} in Figure S6F, all subsets in Figure 6E). IL-7 did trend toward increasing the stem cell memory fraction ($T_{SCM,}$ $CD45RO^-CD45RA^+CD95^+CCR7^+$) compared to IL-2, though changes were non-significant (Figure 6F).

We next evaluated whether IL-7 increased VLA-4 expression on human T cells, as we had seen in our mouse models. We observed a biphasic distribution in VLA-4^+ cells and classed lymphocytes as VLA-4^{Neg}, VLA-4^{Lo} or VLA-4^{Hi} (gating in Figure 6G). For both control and glioblastoma samples, IL-7 significantly increased the VLA-4^{Hi} fraction over that seen with IL-2 (Figure 6H, $p<0.001$***, $CD4^+$ and $CD8^+$ T cell gMFI shown in Figure S6, G & H). Significant upregulation of VLA-4 expression was observed on $CD8^+$ T_{EFF} and $CD8^+$ T_{SCM} subsets from both groups (Figure 6, I and J, $p<0.01$** for healthy controls and $p<0.001$*** for glioblastoma patients). Changes to $CD8^+$ T_{EM} VLA-4 expression were non-significant (Figure S6I).

Finally, we performed in vitro functional assays. These included cytotoxicity assays using our end-expansion product, cultured alongside BRiTE and $EGFRvIII^+$ positive tumor (U87vIII), as described above. Similar dose-dependent tumor killing was observed across all conditions above BRiTE concentrations of 10^3 pg/mL (Figure 6K). We then undertook in vitro stimulation assays of sorted $CD8^+$ T cells (cytokine gating strategy in Figure S7A, sort gating in Figure S7B). Sorted

CD8$^+$ T cells were expanded with IL-2 or IL-7 and co-cultured with tumor only (U87vIII); tumor + BRiTE; or phorbol myristate acetate (PMA)/ionomycin. T cells not exposed to tumor, BRiTE or PMA were also analyzed to assess background activity. We observed similar results for IL-2- and IL-7-expanded glioblastoma patient CD8$^+$ T cells in terms of CD107a^{Hi} degranulation, interferon-gamma (IFN-γ), and tumor-necrosis factor-alpha (TNF-α) production (Figure 6, L-N). While we did observe increased frequencies of Granzyme B$^+$ (GzmB$^+$) T cells in the IL-2-expanded group compared to those expanded with IL-7, we also noted an increased baseline frequency of GzmB$^+$ T cells in the unstimulated / IL-2-expanded and tumor only control groups (Figure 6O). Ultimately, then, IL-7 expansion enhanced CD8$^+$ T cell VLA-4 expression amongst hPBMC samples in a manner similar to that seen with murine T cells, while having a similar impact on T cell function to IL-2 exposure.

IL-7 increases transcription of genes in T cells associated with enhanced migratory function (*CD9*) and protection against sequestration (*S1PR1)*

To evaluate IL-7's effect on migratory integrin expression, we performed bulk RNA sequencing using the same glioblastoma hPBMC samples. CD8$^+$ T cells were sorted from naïve (pre-expansion), IL-2-expanded, or IL-7-expanded products. Principal component analysis revealed that expansion with IL-7 vs. IL-2 resulted in distinct CD8$^+$ T cell transcriptional fates (Figure 7, A-C). Deeper interrogation of these fates via analysis of differential gene expression revealed that IL-7 significantly increases the transcription of genes involved in T cell migration and trafficking compared to IL-2 (*EPHA4* (adjusted p (p_{adj})= 9.39E-27(45)), *ITGA4* (VLA-4, p_{adj}=0.043) and *ITGA6 (*VLA-6, p_{adj}=9.64E-08 (46))). Genes involved in stem-like/memory T cell development were also significantly increased by IL-7 exposure (*TCF7* which encodes for TCF1, p_{adj}=1.60E-06 (47), *FOXO1,* p_{adj}=7.52E-11 and *LEF1*, p_{adj}=2.41E-10). IL-2-expanded CD8$^+$ T cells demonstrated increased transcription of T cell markers associated with effector activity (*CD69,* p_{adj}=2.48E-34*, GZMB,* p_{adj}=2.16E-18) and exhaustion (*CTLA-4,* p_{adj}=1.55E-33, *TOX* p_{adj}=0.00068, *HAVCR2* (TIM-3) p_{adj}=0.00018). Volcano plots for all three comparisons are shown in Figure S8, A and B (naïve vs IL-2 or IL-7, respectively), and Figure 7D (IL-2- vs IL-7-expanded). Analysis of raw transcripts per million (TPM) also found that IL-7 yielded the highest TPM for *ITGA4* (VLA-4), but this was not significantly increased compared to the IL-2 cohort (Figure S8C).

Differential expression analysis also revealed a highly significant outlier when expanding with IL-2 vs IL-7. Transcription of Dual-Specificity Phosphatase 6 (*DUSP6*) was increased 6.8x when expanding with IL-2 vs IL-7 (Figure 7D, p= 7.85E-258). DUSP6 has been shown to negatively regulate the extracellular signal-regulated kinase (ERK1/2) pathway (48-50),

which is activated by IL-2 (51). Curious as to the impact of DUSP6, we performed a repeat 2-week expansion where hPBMCs were expanded with IL-2 alone, or alongside BCI, a small molecule inhibitor of DUSP6 (52). We found that while BCI did not increase $CD8^+$ T cell VLA-4 expression, it did increase the fraction of $CD8^+$ T_{SCM} cells ($CD8^+$ T cell VLA-4 gMFI in Figure S8D, $CD8^+$ T_{SCM} fraction in Figure S8E, technical repeats). We surmised that DUSP6 may affect $CD8^+$ T cell differentiation, but not VLA-4 expression.

Noting that transcription of another migratory integrin (VLA-6) was enhanced with IL-7, we considered whether broader changes in integrin expression might be occurring. We performed hierarchical cluster heatmapping of genes that were differentially expressed across the naïve, IL-2 and IL-7 groups. This identified seven clusters (I-VII, Figure 7E). Clusters I and VI were specifically upregulated in the IL-2-expanded samples, while cluster V was upregulated for both. Cluster IV was the only gene set specifically upregulated within IL-7-expanded samples. To interrogate the biological processes that these clusters represented, we performed Gene Ontology (GO) analysis using the NIH DAVID database (53). For clusters I and VI (upregulated in IL-2), we identified biological processes associated with an inflammatory adaptive immune response and positive regulation of T cell activation (Figure S8, F and G). These included genes related to cytotoxic T cell activity (*GZMA, GZMB, IFNγ, FASLG, CD69*) as well as markers of T cell exhaustion (*CTLA-4, TOX*). For cluster V (upregulated in both), increased transcription of genes associated with cell division were observed (e.g., *MKI67 (54),* Figure S8H).

GO analysis of cluster IV (upregulated in IL-7) identified biological processes associated with positive regulation of cell migration (Figure 7F). These included genes encoding for *ITGA6* (VLA-6, TPM comparisons across groups shown in Figure 7G) as well as *CD9*, a protein that has been associated with increased expression of multiple migratory integrins, including VLA-6 and VLA-4 (55, 56). Within our data, *CD9* TPM was significantly and specifically increased within IL-7 expanded hPBMCs compared to naïve or IL-2 expanded cohorts ($p<0.01$**, Figure 7H). Interestingly, we also identified *S1PR1* (encoding the S1P1 receptor) within cluster IV. Our group has previously reported that loss of S1P1 mediates tumor-induced T cell sequestration in bone marrow (5) and that stabilization of S1P1 on the surface of T cells makes them resistant to sequestration (5). Here, we find that IL-2 significantly reduced *S1PR1* TPM compared to naïve controls ($p<0.05$*), while IL-7 significantly increased *S1PR1* TPM ($p<0.001$***, Figure 7I). We concluded that IL-7 upregulates genes associated with migratory integrin expression, while also increasing *S1PR1* transcription.

Discussion

For T cell-activating therapies to be effective against tumors of the CNS, they must be able to encounter functional immune cells within the intracranial compartment. Although immune cells can cross the BBB (28), primary CNS malignancies are capable of "driving" T cells away by inducing loss of lymphocytic S1P1, resulting in T cell sequestration within bone marrow (5, 57).

Our results demonstrate that non-specific $CD8^+$ T cells expanded with IL-7 can accumulate in tumor tissue, despite tumor-induced T cell sequestration. Further, we demonstrate that the administration of IL-7-ALT can synergize with multiple T cell-activating therapies against established intracranial glioma. Campian et al reported a related phenomenon, whereby peripheral administration of long-acting recombinant IL-7 enhanced cytotoxic $CD8^+$ T cell numbers systemically and in tumor for similar animal glioma models (13). Another recent study by Lee et al. reports synergism between recombinant IL-7 administration and bi-specific T cell engager therapy in solid tumor models (27). Interestingly, they report that IL-7 encourages recruitment of non-exhausted polyclonal bystander $CD8^+$ TILs to tumors. Though these bystander TILs do not have direct anti-tumor activity themselves, they can be redirected by T cell engagers to become tumoricidal. Our study adds to this body of literature, finding that IL-7 enhances expression of migratory integrins like VLA-4, and increases transcription of genes involved in resistance to sequestration (*S1PR1*).

IL-7's effect on upregulating VLA-4 has been previously reported in vitro (58), and peripheral administration of recombinant human IL-7 (rhIL-7) has been observed to increase VLA-4 and T cell trafficking in murine models of sepsis (59). In our study, RNA sequencing of $CD8^+$ T cells from glioblastoma patients similarly identified that transcription of VLA-4 was greatest when expanding with IL-7. Interestingly, while only IL-7 significantly increased $CD8^+$ VLA-4 transcription levels compared to pre-expansion lymphocytes, no significant difference in VLA-4 TPM was observed between IL-2 and IL-7 expanded cells. However, evaluation of genes uniquely upregulated by IL-7 did identify transmembrane proteins *(CD9)* associated with multiple VLA integrins (55, 56). In keeping with this finding, we observed significantly increased transcription of *ITGA6* (VLA-6) when expanding with IL-7 compared to IL-2. Though our study found that VLA-4 was necessary for enhanced $CD8^+$ T cell accumulation, it is possible that IL-7 increases the expression of multiple pro-infiltrative integrins. These could further enhance the ability of $CD8^+$ T cells to enter and accumulate in intracranial glioma.

As mentioned, other genes uniquely upregulated by IL-7 included the g-protein-coupled receptor *S1PR1*. We also have previously identified that S1P1 loss mediates T cell sequestration (5). Accordingly, mice with genetically stabilized S1P1 expression in T cells prove sequestration-resistant and experience prolonged survival to immunotherapy in the face of glioma (5). Our findings align with this prior work. Notably, we also identify that IL-2 exposure decreases the transcription of *S1PR1*. This in turn may underlie some of the failure of IL-2-expanded cellular products to accumulate in intracranial tumors, though further confirmatory work is required.

We also report here increasing lymphocyte VLA-4 expression and increasing numbers of VCAM-1$^+$ endothelial cells/pericytes in the context of glioma over the course of tumor progression. Given that recent studies have reported low fractions of VCAM-1$^+$ cells in other intracranial malignancies (melanoma (41)), this finding suggests that T cell recruitment and BBB trafficking dynamics may vary between cancer types. To identify disease-specific approaches for enhancing T cell accumulation in tumors of the CNS, further evaluation of VCAM-1$^+$ expression across multiple tumor types is warranted. Nevertheless, our findings suggest that for intracranial glioma, VLA-4^{Hi} lymphocytes may be able to encounter VCAM-1 and accumulate in tumor.

To better reflect the capacity for clinical translation, we confirmed that IL-7 exposure upregulated VLA-4 expression on hPBMCs from both healthy donors and patients with glioblastoma. While we observed reduced yields and less CD8$^+$ T cell skewing when expanding hPBMCs with IL-7, we did find that IL-7-cultured hCD8$^+$ T cells exhibited similar in vitro functionality to those being IL-2-cultured. Further optimization could include sorting infiltrative (VLA-4^{Hi}) CD8$^+$ T cells pre-administration. This might also permit administering a reduced dose to patients, or one with more efficient tumor uptake. In our study, the percentage of the administered ALT dose which entered the brain was small, in keeping with other studies evaluating IV CAR-T therapy against murine CNS malignancy models (<1%, lymphoma (60)). Though our approach did not induce overt toxicity/demyelination in brain or spinal cord when combining IL-7-ALT with αPD-1, we did observe a few scattered foci of hepatic cellular apoptosis/necrosis associated with lymphocytic infiltrate. An optimized VLA-4^{Hi} population could reduce the ALT dose required for efficacy, and limit non-CNS organ infiltration.

A key limitation of our study is that we only evaluated the cytokines IL-2 and IL-7, as we have previously established that they can independently support T cell expansion (22). Similarly, we used doses of IL-2 and IL-7 that are known to expand T cells from both mice and humans. However, cytokines such as IL-15, IL-18, IL-21 and others have been used in varying doses to supplement lymphocyte expansion (61). We also note that the IL-7 receptor is downregulated after sustained

exposure, and intermittent cycling with IL-7 may enhance the cytokine's effects (62). Our study is confined to evaluating these two cytokines at the specified concentrations and exposure schedules. However, given the vast number of possible permutations, determining the optimal combination, concentration, and timing for cytokine supplementation is beyond the scope of this manuscript and may require a continuous process-development effort.

In conclusion, we find that expansion of autologous T lymphocytes with IL-7 enhances the ability of $CD8^+$ T cells to accumulate within intracranial glioma, even in the setting of tumor-imposed T cell sequestration. Combination IL-7-ALT and T cell-centric immunotherapies increase survival in multiple models of glioma. Analysis of migratory integrins on lymphocytes finds that IL-7 increases $CD8^+$ T cell expression of VLA-4. RNAseq analysis finds that IL-7 increases transcription of genes associated with increased migratory integrin expression *(CD9)* as well as *S1PR1*, a G protein-coupled receptor whose stable expression on lymphocytes protects against their sequestration. These findings will be used to inform future clinical trials, where ALT pre-treatment will be combined with T cell-activating therapies targeting glioblastoma (e.g., BRiTE, NCT04903795).

Materials and Methods

Sex as a biological variable

For pre-clinical in vivo studies, we exclusively used females as CT-2A was established in female mice (63) and superior engraftment of human hematopoietic stem cells has been observed in female NOD-*scid* gamma (NSG) mice (64). Evaluation of clinical samples from volunteers and glioblastoma patients used hPBMCs from males and females (**Table 1**). Further demographic information in terms of reporting race and ethnicity were based on classifications within the electronic medical records system where available and categorized according to NIH policy (notice number: NOT-OD-15-089).

Mice

All mouse strains used, and housing conditions are described within the Supplemental Methods.

Cell lines

C57BL/6 syngeneic CT2A was originally provided by Robert L. Martuza (Massachusetts General Hospital, Boston, MA, USA). Generation of stably transfected sublines was performed in-house and used in previous studies (1). Similarly, U87MG was obtained from the American Type Culture Collection (ATCC, cat #HTB-14) and transfected in-house to stably express EGFRvIII. GL261 was obtained from the NCI (National Cancer Institute, Frederick, Maryland, USA). Their generation and usage has also been described in prior studies by our group (2). All cell lines are authenticated and confirmed to be contaminant free via IDEXX Laboratories. CT2A, U87MG and GL261 lines were maintained in culture using complete DMEM (Gibco, 11995-065, 10% FBS) and passaged using 0.05% Trypsin, EDTA (Gibco, 25300-054).

Murine lymphocyte culturing

Expansion processes for murine $CD3^+$ cells are described within the Supplemental Methods.

Leukapheresis and human PBMC culturing

Human PBMC collection, processing and expansion are described within the Supplemental Methods.

Tumor inoculation

All tumor studies in this report placed tumors intracranially in mice and followed protocols described previously (65), which are described within the Supplemental Methods.

In vivo adoptive lymphocyte transfer and antibody administration

For adoptive lymphocyte transfer in this study, cells that had been expanded as described in the murine lymphocyte culturing section were administered as described within the Supplemental Methods.

Tissue processing and flow cytometry

Procedures for tissue processing and flow cytometry are based on our previously published protocols (4) and are described within the Supplemental Methods.

Cytotoxicity

Tumor cells were labelled with a viability dye before co-culture. The process is described within the Supplemental Methods.

Immune functional assays

Immune functional assays were performed with flow-sorted human $CD8^+$ T cells and is described within the Supplemental Methods.

Immunohistochemistry & toxicity

Toxicity studies were conducted in C57/Bl6 mice. Processing procedures are described within the Supplemental Methods.

RNA sequencing assays and analysis

Flow-sorted $CD8^+$ T cells were snap frozen in cell pellets and analyzed via bulkRNA sequencing at Azenta life sciences. Analysis is described within the Supplemental Methods. PCA analysis was generated using BioJupies (66). Hierarchical cluster heatmaps were generated via the same method and using clustergrammer (Maayan lab, (67)). Gene Ontology (GO) biological processes analysis was performed using the NIH database for annotation, visualization and integrated

discovery dashboard (DAVID (53)). Volcano plots were generated based on tests for differential expression (Wald test used to generate p-values and log2 fold changes) created with DESeq2 (68) and visualized using VolcaNoseR (69).

Statistics and reproducibility

Experimental results are presented as mean ± SEM unless otherwise stated. Statistical tests for all studies were completed using GraphPad v.10.3.1 (Prism). For comparisons in a single graph, 2-tailed Student's t test or nonparametric Mann-Whitney U test was used, and for multiple comparisons, ANOVA (one-way or two-way) with Holm–Šidák correction for multiple comparisons. Asterisks represent the significance level of any difference (*$p<0.05$, **$p\leq0.01$, ***$p<0.001$, ****$p<0.0001$, $p>0.05$ not significant). Sample sizes were selected due to practical considerations, with no formal power calculations performed. Efficacy studies following animals for survival were assessed for significance using a log-rank (Mantel-Cox) test. Independent study results were pooled if the effect of replication did not cause significant variation as assessed by two-way ANOVA. All animals were randomized within genotype prior to treatment following tumor implantation. Survival was monitored with the assistance of technicians from the Duke Division of Laboratory Animal Resources (DLAR) who were blinded to study groups and followed animals to endpoint.

Study approval

All animal experiments were performed under Duke University IACUC experimental protocol (ID: A163-21-08). Stored anonymized human samples used were collected from glioblastoma patients or volunteers who provided written consent to undergo leukapheresis for T cell expansion for research (glioblastoma donors: Duke IRB #Pro00069444; Duke IRB #Pro00083828; healthy donors: Duke IRB #Pro00009403; approval for secondary analysis: Duke IRB #Pro00117663).

Graphical illustrations

The graphical abstract and experimental outlines in Figs. 1, 2, 3, 5, 6, S1, S3 and S7 were created with BioRender.com and exported under a paid license.

Data Availability

Values for underlying data for all figures are available in the supporting data values file. RNAseq data (processed TPM counts for individual anonymized samples) has been deposited on the NCBI Gene Expression Omnibus (GEO) repository

under accession number GSE288436, available at https://www.ncbi.nlm.nih.gov/geo/query/acc.cgi?acc=GSE288436. Institutional certification for deposition of genomic summary results was granted by Duke's IRB review board.

Author Contributions

Design, acquisition, analysis of data, and writing of manuscript: KS with assistance from KMH, SLC, PN, YZ, EM, COR, EEB, BJP, SEW, PKN, GEA, BHS, KA, JHS, MK and PEF. Overall supervision throughout by JHS, MK and PEF.

Acknowledgements

The authors have been supported by the following grants to Duke University: P50-CA190991 (SPORE) (JHS, MK), P01-CA225622 (JHS, MK), U01-NS090284 (JHS), R01-NS099463 (JHS), R01-CA175517 (JHS), and R01-CA235612 (JHS, MK) as well as a Structured Research Agreement with Adaptin Bio (KS, MK). The authors also wish to express their gratitude to Dr. Rebecca Bacon and Dr. Ivan Spasojevic at Duke University Medical Center for their assistance with toxicity studies.

References

1. Belmontes B, Sawant DV, Zhong W, Tan H, Kaul A, Aeffner F, et al. Immunotherapy combinations overcome resistance to bispecific T cell engager treatment in T cell-cold solid tumors. *Science Translational Medicine.* 2021;13(608):eabd1524.
2. Woroniecka KI, Rhodin KE, Dechant C, Cui X, Chongsathidkiet P, Wilkinson D, et al. 4-1BB Agonism Averts TIL Exhaustion and Licenses PD-1 Blockade in Glioblastoma and Other Intracranial Cancers. *Clinical cancer research : an official journal of the American Association for Cancer Research.* 2020;26(6):1349-58.
3. Baeuerle PA, and Wesche H. T-cell-engaging antibodies for the treatment of solid tumors: challenges and opportunities. *Curr Opin Oncol.* 2022;34(5):552-8.
4. Tomaszewski WH, Waibl-Polania J, Miggelbrink AM, Chakraborty MA, Fecci PE, Sampson JH, et al. Broad immunophenotyping of the murine brain tumor microenvironment. *Journal of Immunological Methods.* 2021;499:113158.
5. Chongsathidkiet P, Jackson C, Koyama S, Loebel F, Cui X, Farber SH, et al. Sequestration of T cells in bone marrow in the setting of glioblastoma and other intracranial tumors. *Nat Med.* 2018;24(9):1459-68.
6. Waibl Polania J, Hoyt-Miggelbrink A, Tomaszewski WH, Wachsmuth LP, Lorrey SJ, Wilkinson DS, et al. Antigen presentation by tumor-associated macrophages drives T cells from a progenitor exhaustion state to terminal exhaustion. *Immunity.* 2024.
7. Maddison K, Graves MC, Bowden NA, Fay M, Vilain RE, Faulkner S, et al. Low tumour-infiltrating lymphocyte density in primary and recurrent glioblastoma. *Oncotarget.* 2021;12(21):2177-87.
8. Reardon DA, Brandes AA, Omuro A, Mulholland P, Lim M, Wick A, et al. Effect of Nivolumab vs Bevacizumab in Patients With Recurrent Glioblastoma: The CheckMate 143 Phase 3 Randomized Clinical Trial. *JAMA Oncology.* 2020;6(7):1003-10.
9. Omuro A, Brandes AA, Carpentier AF, Idbaih A, Reardon DA, Cloughesy T, et al. Radiotherapy combined with nivolumab or temozolomide for newly diagnosed glioblastoma with unmethylated MGMT promoter: An international randomized phase III trial. *Neuro-oncology.* 2023;25(1):123-34.
10. Lim M, Weller M, Idbaih A, Steinbach J, Finocchiaro G, Raval RR, et al. Phase III trial of chemoradiotherapy with temozolomide plus nivolumab or placebo for newly diagnosed glioblastoma with methylated MGMT promoter. *Neuro-oncology.* 2022;24(11):1935-49.

11. Gedeon PC, Schaller TH, Chitneni SK, Choi BD, Kuan CT, Suryadevara CM, et al. A Rationally Designed Fully Human EGFRvIII:CD3-Targeted Bispecific Antibody Redirects Human T Cells to Treat Patient-derived Intracerebral Malignant Glioma. *Clinical cancer research : an official journal of the American Association for Cancer Research.* 2018;24(15):3611-31.

12. Woroniecka K, Chongsathidkiet P, Rhodin K, Kemeny H, Dechant C, Farber SH, et al. T-Cell Exhaustion Signatures Vary with Tumor Type and Are Severe in Glioblastoma. *Clinical cancer research : an official journal of the American Association for Cancer Research.* 2018;24(17):4175-86.

13. Campian JL, Ghosh S, Kapoor V, Yan R, Thotala S, Jash A, et al. Long-Acting Recombinant Human Interleukin-7, NT-I7, Increases Cytotoxic CD8 T Cells and Enhances Survival in Mouse Glioma Models. *Clinical Cancer Research.* 2022;28(6):1229-39.

14. Agliardi G, Liuzzi AR, Hotblack A, De Feo D, Núñez N, Stowe CL, et al. Intratumoral IL-12 delivery empowers CAR-T cell immunotherapy in a pre-clinical model of glioblastoma. *Nature Communications.* 2021;12(1):444.

15. Leonard JP, Sherman ML, Fisher GL, Buchanan LJ, Larsen G, Atkins MB, et al. Effects of single-dose interleukin-12 exposure on interleukin-12-associated toxicity and interferon-gamma production. *Blood.* 1997;90(7):2541-8.

16. Zhang L, Morgan RA, Beane JD, Zheng Z, Dudley ME, Kassim SH, et al. Tumor-infiltrating lymphocytes genetically engineered with an inducible gene encoding interleukin-12 for the immunotherapy of metastatic melanoma. *Clinical cancer research : an official journal of the American Association for Cancer Research.* 2015;21(10):2278-88.

17. Taylor CA, Watson RA, Tong O, Ye W, Nassiri I, Gilchrist JJ, et al. IL7 genetic variation and toxicity to immune checkpoint blockade in patients with melanoma. *Nature Medicine.* 2022;28(12):2592-600.

18. Bagley SJ, Logun M, Fraietta JA, Wang X, Desai AS, Bagley LJ, et al. Intrathecal bivalent CAR T cells targeting EGFR and IL13Rα2 in recurrent glioblastoma: phase 1 trial interim results. *Nature Medicine.* 2024.

19. Choi BD, Gerstner ER, Frigault MJ, Leick MB, Mount CW, Balaj L, et al. Intraventricular CARv3-TEAM-E T Cells in Recurrent Glioblastoma. *New England Journal of Medicine.* 2024.

20. Bagley SJ, Binder ZA, Lamrani L, Marinari E, Desai AS, Nasrallah MP, et al. Repeated peripheral infusions of anti-EGFRvIII CAR T cells in combination with pembrolizumab show no efficacy in glioblastoma: a phase 1 trial. *Nature Cancer.* 2024.

21. O'Rourke DM, Nasrallah MP, Desai A, Melenhorst JJ, Mansfield K, Morrissette JJD, et al. A single dose of peripherally infused EGFRvIII-directed CAR T cells mediates antigen loss and induces adaptive resistance in patients with recurrent glioblastoma. *Sci Transl Med.* 2017;9(399).

22. Yang S, Archer GE, Flores CE, Mitchell DA, and Sampson JH. A cytokine cocktail directly modulates the phenotype of DC-enriched anti-tumor T cells to convey potent anti-tumor activities in a murine model. *Cancer immunology, immunotherapy : CII.* 2013;62(11):1649-62.

23. Ley K, and Kansas GS. Selectins in T-cell recruitment to non-lymphoid tissues and sites of inflammation. *Nature reviews Immunology.* 2004;4(5):325-35.

24. Nolz JC, Starbeck-Miller GR, and Harty JT. Naive, effector and memory CD8 T-cell trafficking: parallels and distinctions. *Immunotherapy.* 2011;3(10):1223-33.

25. Chen D, Tang TX, Deng H, Yang XP, and Tang ZH. Interleukin-7 Biology and Its Effects on Immune Cells: Mediator of Generation, Differentiation, Survival, and Homeostasis. *Front Immunol.* 2021;12:747324.

26. Capitini CM, Chisti AA, and Mackall CL. Modulating T-cell homeostasis with IL-7: preclinical and clinical studies. *J Intern Med.* 2009;266(2):141-53.

27. Lee K-J, Choi D, Tae N, Song HW, Kang Y-W, Lee M, et al. IL-7-primed bystander CD8 tumor-infiltrating lymphocytes optimize the antitumor efficacy of T cell engager immunotherapy. *Cell Reports Medicine.* 2024;5(5).

28. Hickey WF, Hsu BL, and Kimura H. T-lymphocyte entry into the central nervous system. *Journal of Neuroscience Research.* 1991;28(2):254-60.

29. Hinrichs CS, Spolski R, Paulos CM, Gattinoni L, Kerstann KW, Palmer DC, et al. IL-2 and IL-21 confer opposing differentiation programs to CD8+ T cells for adoptive immunotherapy. *Blood.* 2008;111(11):5326-33.

30. Markley JC, and Sadelain M. IL-7 and IL-21 are superior to IL-2 and IL-15 in promoting human T cell–mediated rejection of systemic lymphoma in immunodeficient mice. *Blood.* 2010;115(17):3508-19.

31. Oh T, Fakurnejad S, Sayegh ET, Clark AJ, Ivan ME, Sun MZ, et al. Immunocompetent murine models for the study of glioblastoma immunotherapy. *J Transl Med.* 2014;12:107.

32. Tritz ZP, Ayasoufi K, Malo C, Himes B, Khadka R, Yokanovich L, et al. Combination immunotherapy of αPD-1 and extended half-life IL-2 clears established GL261 gliomas in an MHC class I independent fashion. *The Journal of Immunology.* 2020;204(1 Supplement):169.15-.15.

33. Ayasoufi K, Pfaller CK, Evgin L, Khadka RH, Tritz ZP, Goddery EN, et al. Brain cancer induces systemic immunosuppression through release of non-steroid soluble mediators. *Brain.* 2020;143(12):3629-52.

34. Choi BD, Kuan C-T, Cai M, Archer GE, Mitchell DA, Gedeon PC, et al. Systemic administration of a bispecific antibody targeting EGFRvIII successfully treats intracerebral glioma. *Proceedings of the National Academy of Sciences.* 2013;110(1):270-5.

35. Noffsinger B, Witter A, Sheybani N, Xiao A, Manigat L, Zhong Q, et al. Technical choices significantly alter the adaptive immune response against immunocompetent murine gliomas in a model-dependent manner. *J Neurooncol.* 2021;154(2):145-57.

36. Kohlmeier JE, Miller SC, Smith J, Lu B, Gerard C, Cookenham T, et al. The chemokine receptor CCR5 plays a key role in the early memory CD8+ T cell response to respiratory virus infections. *Immunity.* 2008;29(1):101-13.

37. Ray SJ, Franki SN, Pierce RH, Dimitrova S, Koteliansky V, Sprague AG, et al. The collagen binding alpha1beta1 integrin VLA-1 regulates CD8 T cell-mediated immune protection against heterologous influenza infection. *Immunity.* 2004;20(2):167-79.

38. Savino W, Chaves B, Bonomo AC, and Cotta-de-Almeida V. Integrin-directed antibody-based immunotherapy: focus on VLA-4. *Immunotherapy Advances.* 2021;1(1).

39. Das S, and Marsden PA. Angiogenesis in glioblastoma. *The New England journal of medicine.* 2013;369(16):1561-3.

40. Singh K, Hotchkiss KM, Patel KK, Wilkinson DS, Mohan AA, Cook SL, et al. Enhancing T Cell Chemotaxis and Infiltration in Glioblastoma. *Cancers (Basel).* 2021;13(21).

41. Messmer JM, Thommek C, Piechutta M, Venkataramani V, Wehner R, Westphal D, et al. T lymphocyte recruitment to melanoma brain tumors depends on distinct venous vessels. *Immunity.* 2024;57(11):2688-703.e11.

42. Sehr T, Proschmann U, Thomas K, Marggraf M, Straube E, Reichmann H, et al. New insights into the pharmacokinetics and pharmacodynamics of natalizumab treatment for patients with multiple sclerosis, obtained from clinical and in vitro studies. *Journal of Neuroinflammation.* 2016;13(1):164.

43. Mittelbrunn M, Molina A, Escribese MM, Yáñez-Mó M, Escudero E, Ursa Á, et al. VLA-4 integrin concentrates at the peripheral supramolecular activation complex of the immune synapse and drives T helper 1 responses. *Proceedings of the National Academy of Sciences.* 2004;101(30):11058-63.

44. Miao H, Choi BD, Suryadevara CM, Sanchez-Perez L, Yang S, De Leon G, et al. EGFRvIII-specific chimeric antigen receptor T cells migrate to and kill tumor deposits infiltrating the brain parenchyma in an invasive xenograft model of glioblastoma. *PLoS One.* 2014;9(4):e94281.

45. Holen HL, Nustad K, and Aasheim HC. Activation of EphA receptors on CD4+CD45RO+ memory cells stimulates migration. *J Leukoc Biol.* 2010;87(6):1059-68.

46. Kitayama J, Ikeda S, Kumagai K, Saito H, and Nagawa H. α6β1 Integrin (VLA-6) Mediates Leukocyte Tether and Arrest on Laminin under Physiological Shear Flow. *Cellular Immunology.* 2000;199(2):97-103.

47. Escobar G, Mangani D, and Anderson AC. T cell factor 1: A master regulator of the T cell response in disease. *Sci Immunol.* 2020;5(53).

48. Johnson GL, and Lapadat R. Mitogen-activated protein kinase pathways mediated by ERK, JNK, and p38 protein kinases. *Science.* 2002;298(5600):1911-2.

49. Yoo DH, Im YS, Oh JY, Gil D, and Kim Y-O. DUSP6 is a memory retention feedback regulator of ERK signaling for cellular resilience of human pluripotent stem cells in response to dissociation. *Scientific Reports.* 2023;13(1):5683.

50. Caunt CJ, and Keyse SM. Dual-specificity MAP kinase phosphatases (MKPs). *The FEBS Journal.* 2013;280(2):489-504.

51. Yu T-K, Caudell EG, Smid C, and Grimm EA. IL-2 Activation of NK Cells: Involvement of MKK1/2/ERK But Not p38 Kinase Pathway1. *The Journal of Immunology.* 2000;164(12):6244-51.

52. Kong T, Laranjeira ABA, Yang K, Fisher DAC, Yu L, Poittevin De La Frégonnière L, et al. DUSP6 mediates resistance to JAK2 inhibition and drives leukemic progression. *Nature Cancer.* 2023;4(1):108-27.

53. Sherman BT, Hao M, Qiu J, Jiao X, Baseler MW, Lane HC, et al. DAVID: a web server for functional enrichment analysis and functional annotation of gene lists (2021 update). *Nucleic Acids Res.* 2022;50(W1):W216-w21.

54. Uxa S, Castillo-Binder P, Kohler R, Stangner K, Müller GA, and Engeland K. Ki-67 gene expression. *Cell Death & Differentiation.* 2021;28(12):3357-70.

55. Rubinstein E, le Naour F, Billard M, Prenant M, and Boucheix C. CD9 antigen is an accessory subunit of the VLA integrin complexes. *European Journal of Immunology.* 1994;24(12):3005-13.

56. Scherberich A, Moog S, Haan-Archipoff G, Azorsa DO, Lanza F, and Beretz A. Tetraspanin CD9 Is Associated With Very Late–Acting Integrins in Human Vascular Smooth Muscle Cells and Modulates Collagen Matrix Reorganization. *Arteriosclerosis, Thrombosis, and Vascular Biology.* 1998;18(11):1691-7.

57. Mrdjen D, Pavlovic A, Hartmann FJ, Schreiner B, Utz SG, Leung BP, et al. High-Dimensional Single-Cell Mapping of Central Nervous System Immune Cells Reveals Distinct Myeloid Subsets in Health, Aging, and Disease. *Immunity.* 2018;48(2):380-95.e6.

58. Kitazawa H, Muegge K, Badolato R, Wang JM, Fogler WE, Ferris DK, et al. IL-7 activates alpha4beta1 integrin in murine thymocytes. *The Journal of Immunology.* 1997;159(5):2259-64.

59. Unsinger J, McGlynn M, Kasten KR, Hoekzema AS, Watanabe E, Muenzer JT, et al. IL-7 Promotes T Cell Viability, Trafficking, and Functionality and Improves Survival in Sepsis. *The Journal of Immunology.* 2010;184(7):3768-79.

60. Mulazzani M, Fräßle SP, von Mücke-Heim I, Langer S, Zhou X, Ishikawa-Ankerhold H, et al. Long-term in vivo microscopy of CAR T cell dynamics during eradication of CNS lymphoma in mice. *Proceedings of the National Academy of Sciences.* 2019;116(48):24275-84.

61. Xu XJ, Song DG, Poussin M, Ye Q, Sharma P, Rodríguez-García A, et al. Multiparameter comparative analysis reveals differential impacts of various cytokines on CART cell phenotype and function ex vivo and in vivo. *Oncotarget.* 2016;7(50):82354-68.

62. Vranjkovic A, Crawley AM, Gee K, Kumar A, and Angel JB. IL-7 decreases IL-7 receptor alpha (CD127) expression and induces the shedding of CD127 by human CD8+ T cells. *Int Immunol.* 2007;19(12):1329-39.

63. Martínez-Murillo R, and Martínez A. Standardization of an orthotopic mouse brain tumor model following transplantation of CT-2A astrocytoma cells. *Histol Histopathol.* 2007;22(12):1309-26.

64. Notta F, Doulatov S, and Dick JE. Engraftment of human hematopoietic stem cells is more efficient in female NOD/SCID/IL-2Rgc-null recipients. *Blood.* 2010;115(18):3704-7.

65. Schaller TH, Snyder DJ, Spasojevic I, Gedeon PC, Sanchez-Perez L, and Sampson JH. First in human dose calculation of a single-chain bispecific antibody targeting glioma using the MABEL approach. *J Immunother Cancer.* 2020;8(1).

66. Torre D, Lachmann A, and Ma'ayan A. BioJupies: Automated Generation of Interactive Notebooks for RNA-Seq Data Analysis in the Cloud. *Cell Systems.* 2018;7(5):556-61.e3.

67. Fernandez NF, Gundersen GW, Rahman A, Grimes ML, Rikova K, Hornbeck P, et al. Clustergrammer, a web-based heatmap visualization and analysis tool for high-dimensional biological data. *Scientific Data.* 2017;4(1):170151.

68. Love MI, Huber W, and Anders S. Moderated estimation of fold change and dispersion for RNA-seq data with DESeq2. *Genome Biology.* 2014;15(12):550.

69. Goedhart J, and Luijsterburg MS. VolcaNoseR is a web app for creating, exploring, labeling and sharing volcano plots. *Scientific Reports.* 2020;10(1):20560.

Tables

Table 1. Demographics of hPBMC samples taken from healthy volunteers and glioblastoma patients

Characteristics	Control	Glioblastoma
	N = 5	N = 6
Age (yr)		
Median	54.3 (43.3–55.4)	58.7 (37.4–63.3)
Sex		
Male	2/5 (40%)	4/6 (66%)
Female	1/5 (20%	2/6 (33%)
Unknown	2/5 (40%)	0
Ethnicity		
American Indian/Alaska Native	0	0
Black or African American	0	0
Hispanic or Latino	0	0
Native Hawaiian or other Pacific Islander	0	0
Caucasian	3/5 (60%)	6/6 (100%)
Unknown	2/5 (40%)	0
Diagnosis		
IDHwt* glioblastoma	NA	6/6 (100%)
Newly diagnosed	NA	4/6 (66.7%)
Recurrent	NA	2/6 (33.3%)
Steroid Status		
Naïve	NA	1/6 (16.7%)
Experienced	NA	5/6 (83.3%)

*IDHwt: Isocitrate Dehydrogenase wild-type

Figures

Figure 1. IL-7-ALT CD8⁺ cells demonstrate increased accumulation within orthotopic glioblastoma models despite endogenous T cell sequestration in bone marrow

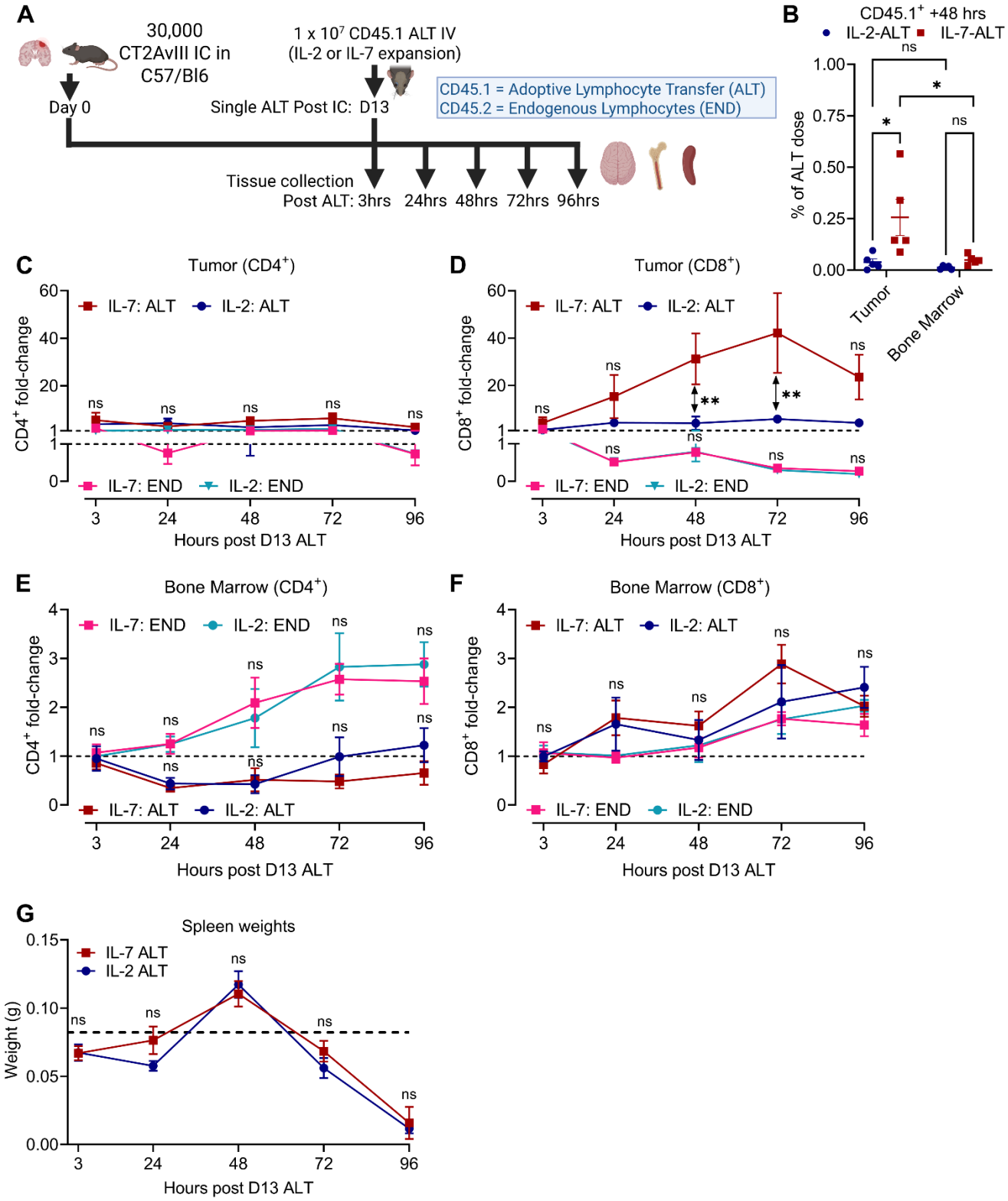

(A) Study overview (n=4-5 mice/group/time point for all graphs).

(B) Percentage of IL-2-ALT and IL-7-ALT CD45.1$^+$ dose detected in tumor by 48-hours post administration (CD4$^+$ & CD8$^+$ T cells).

(C) Fold-change relative to Day 0 of exogenous CD45.1$^+$CD4$^+$ T cell entry and **(D)** CD45.1$^+$CD8$^+$ T cell entry into brain tumors.

(E) Fold-change relative to Day 0 of exogenous CD45.1$^+$CD4$^+$ T cell entry and **(F)** CD45.1$^+$CD8$^+$ T cell entry into bone marrow.

(G) Time course of spleen sizes following ALT. Weights from control mice represented by dashed line (0.0823g, n=5).

Dashed line in C-F represents baseline (i.e., 1x). Statistical analyses performed via two-way ANOVA and data presented as mean ± SEM unless otherwise specified. Experimental outline generated using BioRender.com.

Figure 2. IL-7-ALT synergizes with specific and non-specific T cell-activating/checkpoint blockade therapies in orthotopic glioma models

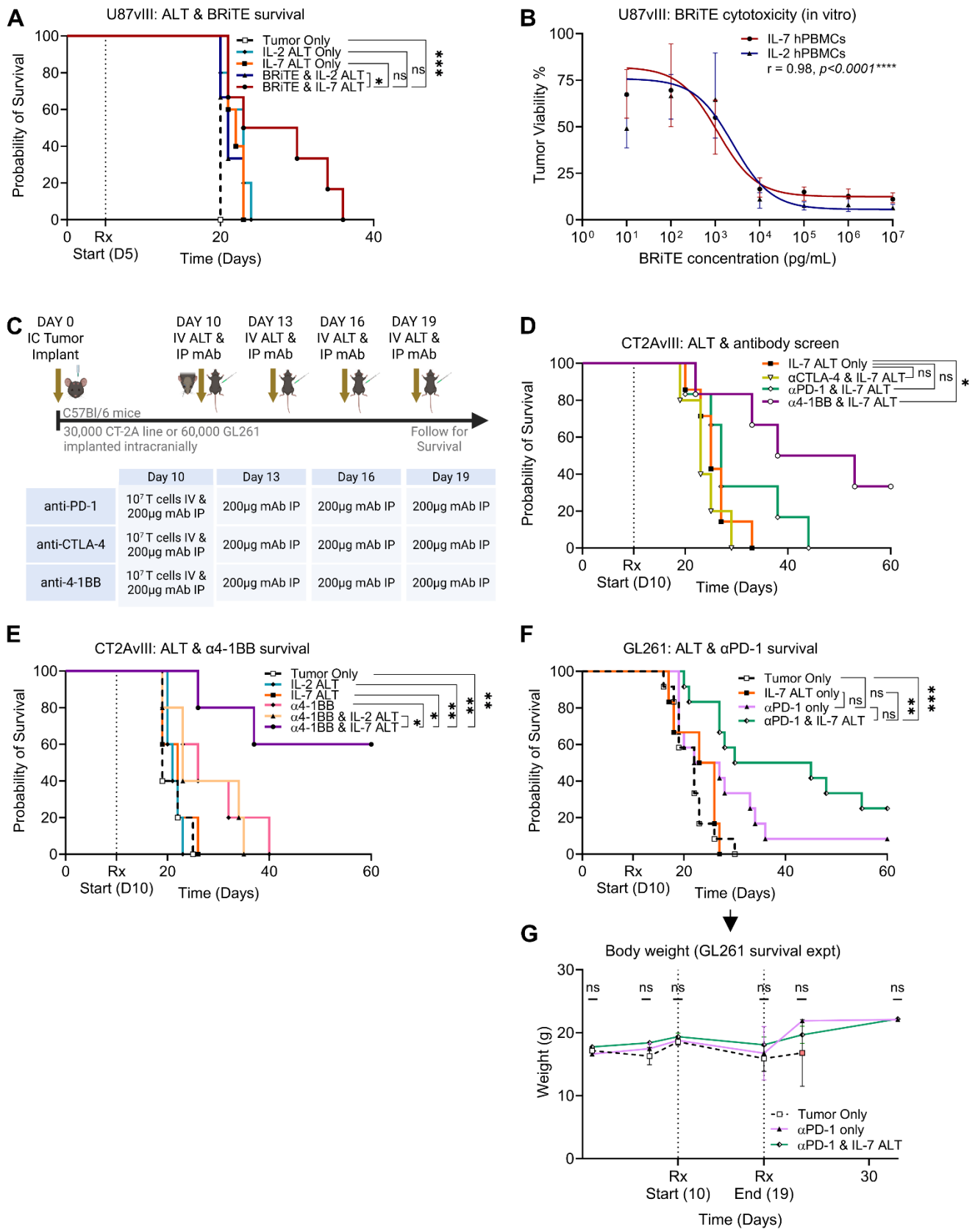

(A) Evaluation of IL-7 and IL-2 ALT combined with hCD3:EGFRvIII BRiTE in NSG mice. Mice (n=5-6 /group) were implanted with U87vIII and treated with 5 x 10^6 IV hPBMCs on day 5, with serial IV BRiTE (50µg) on days 5-9.

(B) Cytotoxicity assay using BRiTE co-cultured with tumor cells (U87vIII) and hPBMCs expanded with IL-2 or IL-7. Non-linear fitted dose-response curves shown with SEM (n=10-12/group, Pearson Correlation Coefficient r = 0.98, p<0.0001****).

(C & D) Study overview and findings of a screening approach to identify the best combinatorial mAb approach with ALT (n=5-7/group).

(E) Survival of combination α4-1BB & IL-7 ALT therapy compared to monotherapy controls treated using same regimen in **(C)** (n=5/group).

(F) C57BL/6 mice implanted with 6 x 10^4 GL261 and treated using same regimen in **(C)** with αPD-1 (n=6-12/group, pooled data across two experiments).

(G) Monitoring of bodyweight throughout the treatment period and for two weeks after for survival experiment in **(F)** (n=6-7/group). Comparison via multiple unpaired t-tests and data presented as mean ± SEM.

Survival comparisons performed via Chi-Squared test. Experimental outlines generated using BioRender.com.

Figure 3. IL-7-expanded CD8⁺ T cells accumulating in tumor consist of both central and effector memory phenotypes

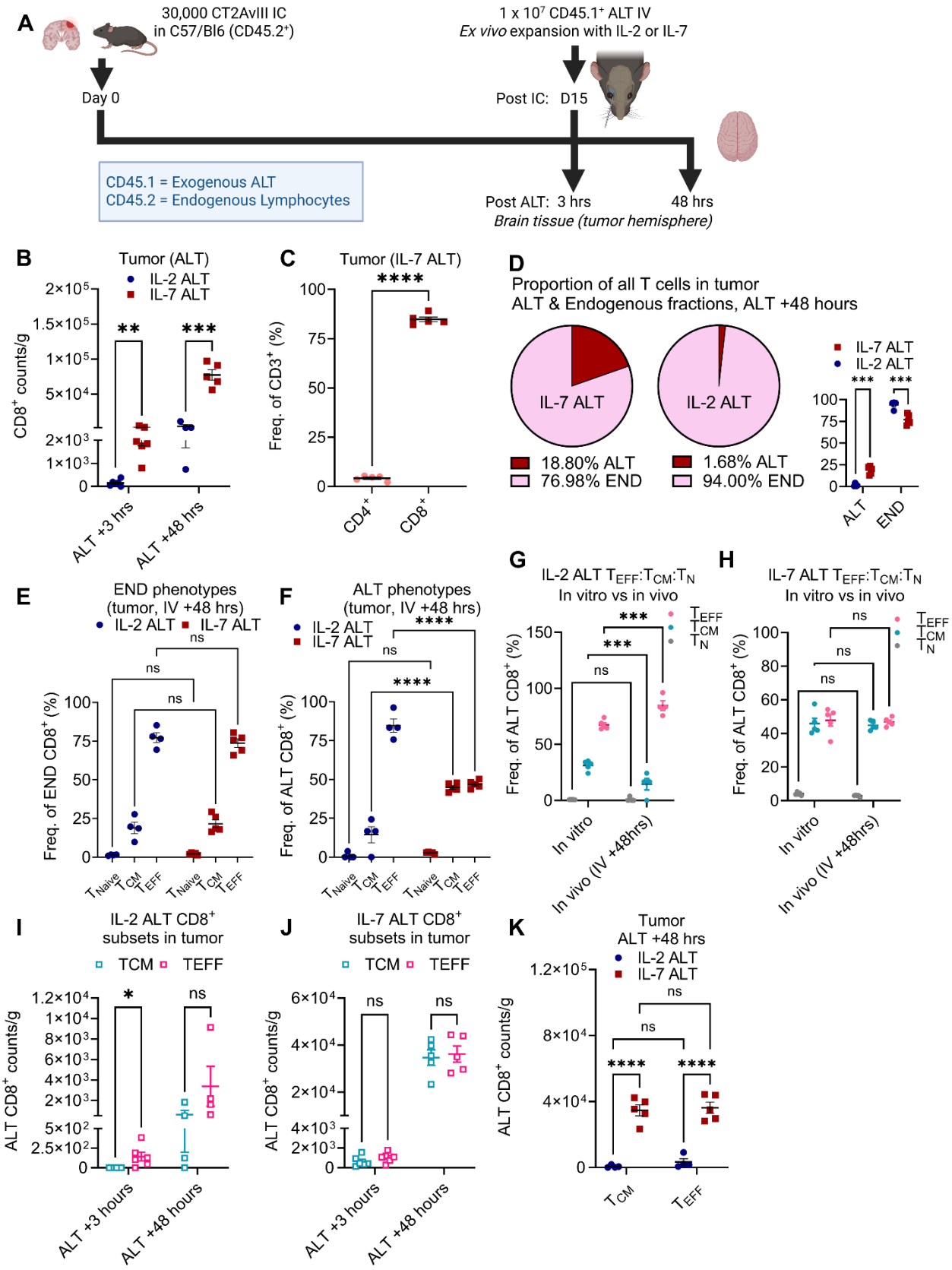

(A) Study overview in C57BL/6 mice (n=4-6/group for all graphs).

(B) Weight-adjusted counts of $CD45.1^+CD8^+$ T cells 3- and 48-hours following ALT in tumor (multiple unpaired t-tests shown).

(C) Proportion of IL-7-ALT cells in tumor that are $CD4^+$ or $CD8^+$ T cells (unpaired t-test).

(D) Proportions of exogenous ALT to endogenous T cells in tumor 48-hours following administration, with paired dot-plot showing individual values across groups.

(E) Comparison of Endogenous ($CD45.2^+$) or exogenous/ALT ($CD45.1^+$) **(F)** $CD8^+$ T_N, T_{CM}, T_{EFF} proportions between IL-2 and IL-7 ALT in tumor 48-hours following administration.

(G & H) Comparison of IL-2 and IL-7 ALT phenotype fractions in tumor to ALT pre-administration.

(I & J) Weight normalized counts at both 3- and 48-hr timepoints of $CD8^+$ T_{CM} and $CD8^+$ T_{EFF} accumulation in tumor when treating with IL-2 or IL-7 ALT (multiple unpaired t-tests shown).

(K) Comparison of $CD8^+$ T_{CM} and $CD8^+$ T_{EFF} presence in tumor following IL-2-ALT or IL-7-ALT.

Statistical analyses performed via two-way ANOVA and data presented as mean ± SEM unless otherwise specified. Experimental outline generated using BioRender.com.

Figure 4. Expansion with IL-7 upregulates expression of the pro-migratory integrin VLA-4 on murine CD8⁺ T cells, which is required for enhanced intra-tumoral accumulation

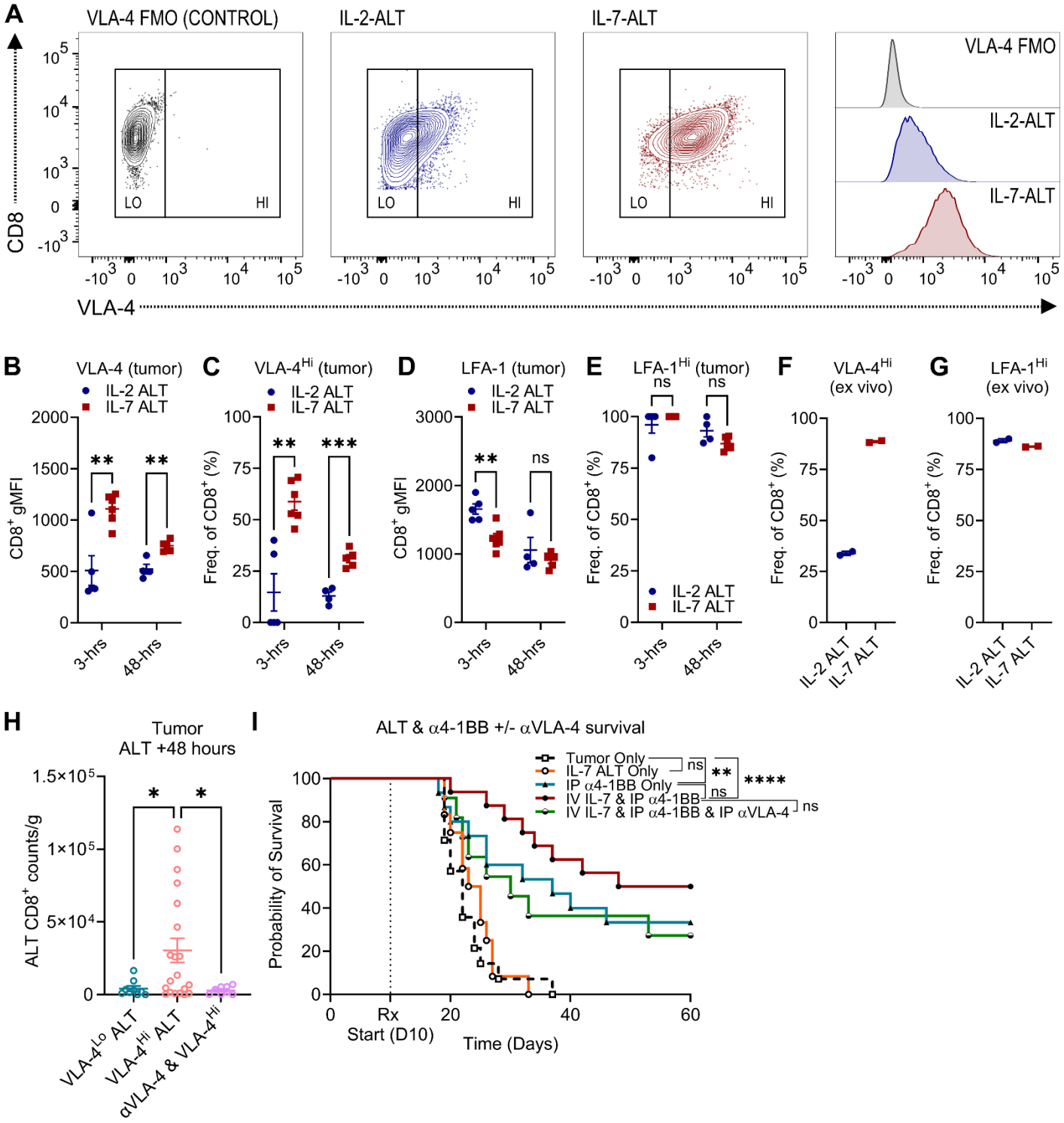

(A) Representative gating strategy shown for VLA-4 expression on $CD8^+$ T cells from IL-2 or IL-7 ALT.

(B & C) $CD8^+$ T cell VLA-4 expression (gMFI) and proportion of $CD8^+$ VLA-4^{Hi} T cells shown when expanding with IL-2 or IL-7 ALT (experiment outline in Figure 3, n=4-6/group).

(D & E) $CD8^+$ T cell LFA-1 expression (gMFI) and proportion of $CD8^+$ LFA-1^{Hi} T cells shown when expanding with IL-2 or IL-7 ALT.

(F & G) Analysis of the $CD8^+$ T cell VLA-4^{Hi} or LFA-1^{Hi} proportion in ALT cellular product at expansion end (2 technical replicates).

(H) Entry of $CD45.1^+CD8^+$ T cells in tumor following VLA-4^{Lo}, VLA-4^{Hi} ALT or VLA-4^{Hi} ALT & αVLA-4 (single-dose 200µg intraperitoneal αVLA-4 antibody (BioXCell) pre-ALT, 3 pooled experiments shown, n=8-20/group, one-way ANOVA shown).

(I) Evaluation of VLA-4 expression on the endogenous $CD8^+$ T cell compartment over time (IL-2 and IL-7 treatment groups pooled, n=9-12/group). Survival comparisons performed via Chi-Squared test.

Statistical analyses performed using unpaired T tests and data presented as mean ± SEM unless otherwise specified.

Figure 5. Lymphocytic VLA-4 & endothelial/pericytic VCAM-1 expression increases over time on native T cells in murine glioma

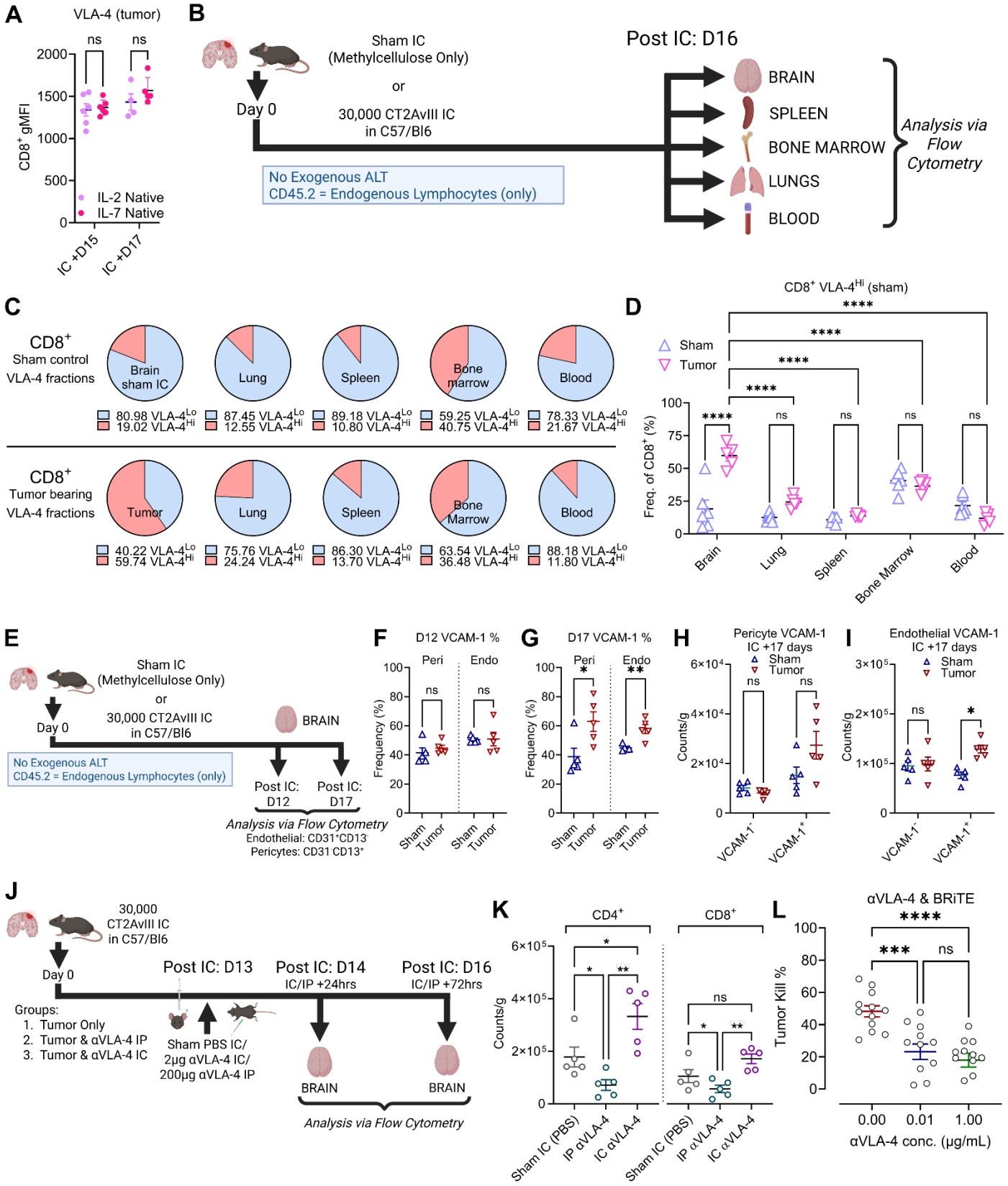

(A) Comparison of $CD8^+$ T cell VLA-4 gMFI expression on endogenous cells over time from prior experiment (n=4-6/group).

(B) Study overview to assess VLA-4 expression across compartments.

(C & D) Evaluation of VLA-4^{Lo} and VLA-4^{Hi} fractions across different compartments. Comparisons in **D** via two-way ANOVA (n=5-6/group).

(E) Study overview to assess endothelial VCAM-1 in the CNS. No ALT was used. Tumor hemispheres were collected, and endothelial cells ($CD31^+CD13^-$)/pericytes ($CD31^-CD13^+$) were analyzed (n=5/group).

(F & G) Frequency of VCAM-1^+ pericytes/endothelial cells in tumor at D12 and D17 following tumor/sham injection.

(H & I) Counts of VCAM-1^-/VCAM-1^+ pericytes/endothelial cells in tumor compared to sham controls at D17 following intracranial injections.

(J) Study overview to evaluate intraperitoneal/intracranial VLA-4 blockade (n=5/group).

(K) Intracranial $CD4^+$ & $CD8^+$ T cell counts 72-hours following administration of intraperitoneal/intracranial αVLA-4 or sham controls. Comparisons via one-way ANOVA.

(L) In vitro cytotoxicity with CT2AvIII, T cells, αVLA-4 and BRiTE at EC_{50} concentration of 0.01μg/mL. n=12/dose level. Comparisons via one-way ANOVA.

Statistical analyses performed using unpaired T tests and data presented as mean ± SEM unless otherwise specified. Experimental outlines generated using BioRender.com.

Figure 6. IL-7 expansion of hPBMCs from both healthy volunteers and patients with glioblastoma upregulates lymphocytic VLA-4 expression

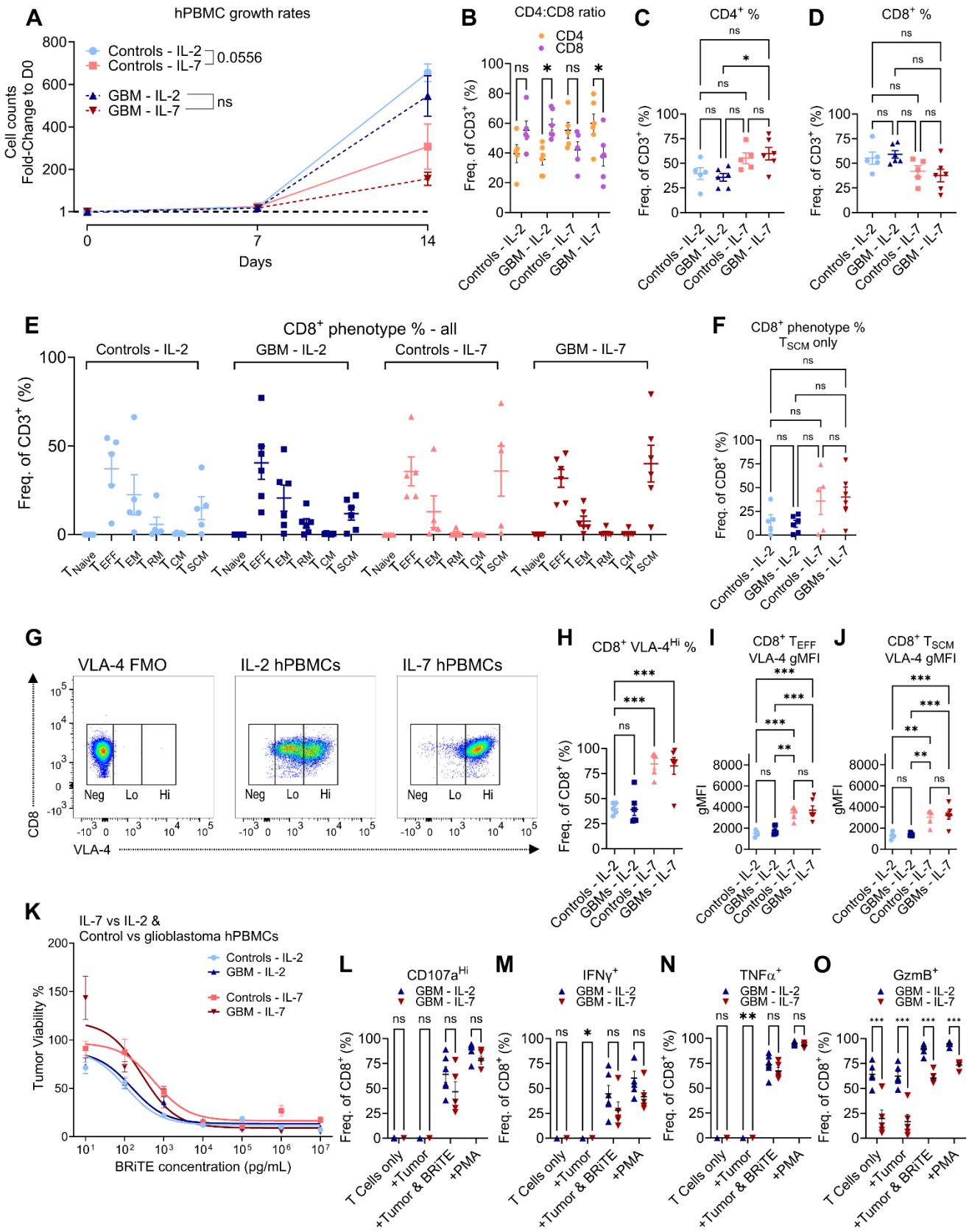

(A) hPBMC growth rates for IL-2 vs IL-7 co-culture from both glioblastoma and control volunteer leukaphereses. (n=5-6/group).

(B-D) $CD4^+$:$CD8^+$ T cell ratios and comparisons for IL-2 vs IL-7 for control and glioblastoma samples at expansion end. **C** & **D**. Comparisons in B via two-way ANOVA and in C & D via one-way ANOVA.

(E) Overview of $CD8^+$ T cell phenotype fractions at expansion end: Naïve (T_N), Effector (T_{EFF}), Effector Memory (T_{EM}), Resident Memory (T_{RM}), Central Memory (T_{CM}), Stem Cell Memory (T_{SCM}).

(F) Fraction of $CD8^+$ T_{SCM} at expansion end across groups.

(G-J) Gating strategy for VLA-4^{Hi} fraction and proportion of VLA-4^{Hi} in all $CD8^+$ T cells (**H**) as well as $CD8^+$ T_{EFF} (**I**) and $CD8^+$ T_{SCM} cells (**J**) at expansion end.

(K) Cytotoxicity assay with tumor (U87vIII) co-cultured with IL-2 or IL-7 expanded donor/glioblastoma hPBMCs & BRiTE.

(L-O) Degranulation assays assessing $CD107^{Hi}$, $GzmB^+$, $IFN\gamma^+$, $TNF\alpha^+$ in glioblastoma $CD8^+$ T cells expanded with IL-2 and IL-7. Comparisons via multiple unpaired t tests (n=5-6/group).

Statistical analyses performed using one-way ANOVA and data presented as mean ± SEM unless specified.

Figure 7. IL-7 upregulates transcription of genes associated with enhanced migratory integrin expression (*CD9*) and protection against tumor-induced sequestration (*S1PR1*)

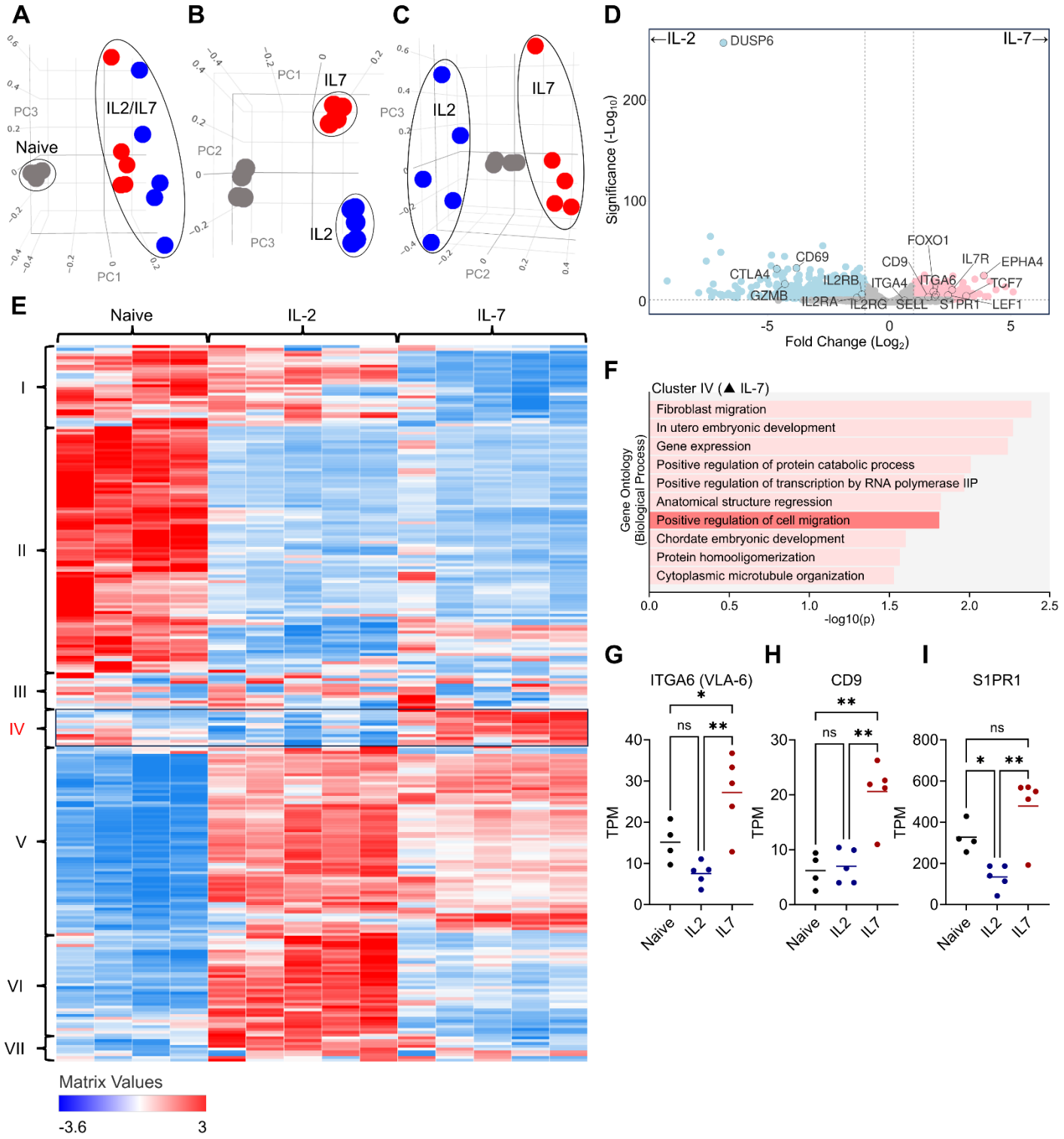

(A-C) Principal component analysis of naïve (grey), IL-2 expanded (blue) and IL-7 expanded (red) $CD8^+$ T cells (n=4-5/group for all graphs).

(D) Volcano plot comparing differential gene expression between IL-2 and IL-7 expanded $CD8^+$ T cells.

(E) Hierarchical cluster heatmaps of the naïve, IL-2 and IL-7 groups with seven unique clusters identified (I-VII).

(F) Gene Ontology biological processes analysis of genes expressed in cluster IV (upregulated with IL-7, *EPHA4, CD9, ITGA6, S1PR1* etc.)

(G-I) Comparisons of raw transcripts per million (TPM) across groups for *ITGA6, CD9* and *S1PR1* (comparisons via one-way ANOVA).

PCA analysis was generated using BioJupies (66). Hierarchical cluster heatmaps were generated using clustergrammer (Maayan lab, (67)). Gene Ontology (GO) biological processes analysis was performed using the NIH DAVID database (53). Volcano plots were generated using VolcaNoseR (69). Comparisons via one-way ANOVA and data presented as mean ± SEM unless otherwise specified.